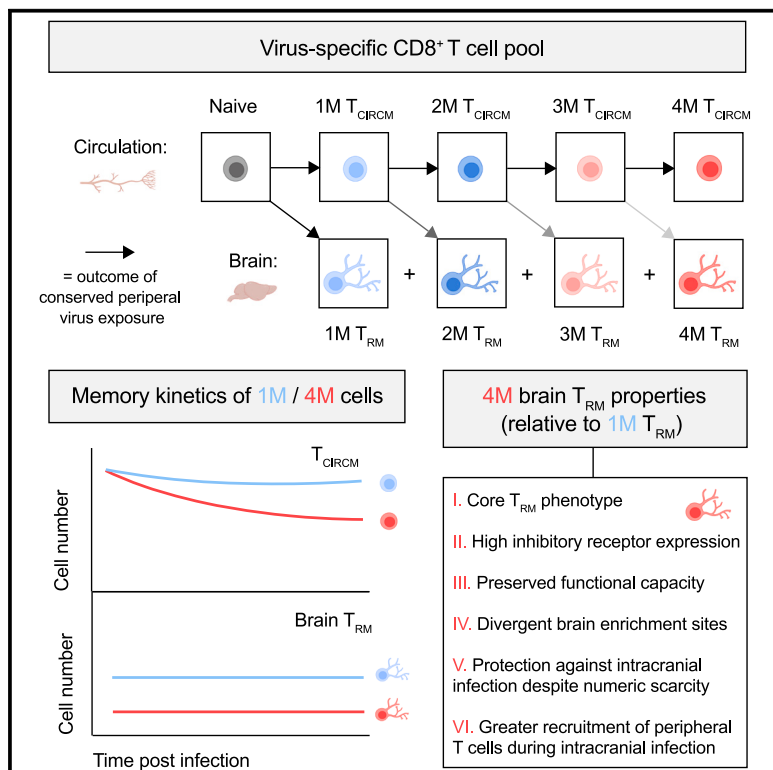


## Repetitive antigen stimulation in the periphery dictates the composition and recall responses of brain-resident memory CD8<sup>+</sup> T cells

### Graphical abstract



### Authors

Madison R. Mix, Stephanie van de Wall,  
Mohammad Heidarian, ...,  
Cassie M. Sievers, Vladimir P. Badovinac,  
John T. Harty

### Correspondence

john-harty@uiowa.edu

### In brief

The impact of repeated peripheral viral infection on brain-resident adaptive immune cells is poorly understood. Utilizing mouse models of repetitive viral infection, Mix et al. demonstrate that prior antigen stimulation history dictates the composition, function, localization, and recall responses of anti-viral brain T<sub>RM</sub>.

### Highlights

- Tissue-resident memory (T<sub>RM</sub>) CD8<sup>+</sup> T cells populate the brain
- Brain T<sub>RM</sub> can be generated by peripheral viral infections
- Repetitive viral stimulation shapes brain T<sub>RM</sub> composition, location, and function
- Repetitively stimulated brain T<sub>RM</sub> can protect against intracranial infection



## Article

# Repetitive antigen stimulation in the periphery dictates the composition and recall responses of brain-resident memory CD8<sup>+</sup> T cells

Madison R. Mix,<sup>1,2,3</sup> Stephanie van de Wall,<sup>1</sup> Mohammad Heidarian,<sup>1,4</sup> Elizabeth A. Escue,<sup>1,4</sup> Cori E. Fain,<sup>1</sup> Lecia L. Pewe,<sup>1</sup> Lisa S. Hancox,<sup>1</sup> Sahaana A. Arumugam,<sup>1,2,3</sup> Cassie M. Sievers,<sup>1</sup> Vladimir P. Badovinac,<sup>1,2,3,4,5</sup> and John T. Harty<sup>1,2,3,4,5,6,\*</sup>

<sup>1</sup>Department of Pathology, Carver College of Medicine, University of Iowa, Iowa City, IA 52242, USA

<sup>2</sup>Medical Scientist Training Program, Carver College of Medicine, University of Iowa, Iowa City, IA 52242, USA

<sup>3</sup>Interdisciplinary Graduate Program in Immunology, Carver College of Medicine, University of Iowa, Iowa City, IA 52242, USA

<sup>4</sup>Experimental Pathology Graduate Program, Carver College of Medicine, University of Iowa, Iowa City, IA 52242, USA

<sup>5</sup>These authors contributed equally

<sup>6</sup>Lead contact

\*Correspondence: john-harty@uiowa.edu

<https://doi.org/10.1016/j.celrep.2025.115247>

## SUMMARY

The human brain harbors virus-specific, tissue-resident memory ( $T_{RM}$ ) CD8<sup>+</sup> T cells. However, the impact of repeated peripheral viral infection on the generation, phenotype, localization, and recall responses of brain  $T_{RM}$  remains elusive. Here, utilizing two murine models of peripheral viral infection, we demonstrate that circulating memory CD8<sup>+</sup> T cells with previous antigen exposure exhibit a markedly reduced capacity to form brain  $T_{RM}$  compared to naive CD8<sup>+</sup> T cells. Repetitively stimulated brain  $T_{RM}$  also demonstrate differential inhibitory receptor expression, preserved functionality, and divergent localization patterns compared to primary memory counterparts. Despite these differences, repetitively stimulated brain  $T_{RM}$  provide similar protection against intracranial infection as primary populations with superior recall-based recruitment of peripheral lymphocytes. As CD8<sup>+</sup> T cells may distinctly seed the brain with each repeated infection of the same host, these findings point to heterogeneity in the brain  $T_{RM}$  pool that is dictated by prior peripheral antigen stimulation history.

## INTRODUCTION

In contrast to historical concepts of immune privilege, the human brain harbors immune cells with innate and adaptive capacities.<sup>1–6</sup> While perturbations in brain immune populations have been extensively studied following central nervous system (CNS) infections, the neuroinflammatory consequences of peripheral infections remain to be fully characterized.<sup>6–19</sup> Recently, peripheral infection models of SARS-CoV-2 and influenza A virus in mice have revealed long-standing alterations in myeloid- and CNS-lineage cell types even in the absence of direct neurotropism.<sup>20</sup> While these studies have been illuminating, a gap in knowledge has arisen in how adaptive immune populations in the brain are impacted by peripheral viral exposure. Furthermore, while the seasonal and repetitive nature of viral infection is widely appreciated among human populations, few published studies address the immunological consequences of recurring viral infection with repetitive antigen stimulation in animal models.<sup>21–32</sup> As a result, the collective impact of repeated viral antigen exposure on brain adaptive immunity remains untested.

CD8<sup>+</sup> T cells establish diverse memory populations after viral infection.<sup>33–37</sup> Following expansion and contraction, these long-lived cells continuously surveil the body as circulating

memory T cells ( $T_{CIRCM}$ ) or permanently embed in organs as tissue-resident memory T cells ( $T_{RM}$ ).<sup>33–37</sup> Even in the absence of CNS infection, peripheral virus-specific  $T_{RM}$  populate the murine brain.<sup>6,13,30,38–40</sup> Similarly, human brain tissue harbors memory CD8<sup>+</sup> T cells with T cell receptors (TCRs) specific for peripheral pathogens such as influenza virus, Cytomegalovirus, and Epstein-Barr virus.<sup>38,41,42</sup> While brain  $T_{RM}$  originally generated from naive T cells have been queried in mice after a single viral exposure, the ability of existing  $T_{CIRCM}$  to form new brain  $T_{RM}$  populations upon a second, third, or fourth peripheral viral exposure is unknown. Thus, the composite memory CD8<sup>+</sup> T cell pool in the brain of mice and/or humans may exhibit heterogeneity based on prior peripheral antigen stimulation history. Critically, these phenotypes cannot be extracted from studies of single viral infections in mice.

Prior investigations have demonstrated that repeated viral exposure can modulate the memory T cell pool outside of the brain. We have previously demonstrated that influenza-specific memory CD8<sup>+</sup> T cells in the lung, mediastinal lymph node (mLN), and spleen of mice exhibit profound numeric, phenotypic, functional, and protective differences based on their history of prior antigen stimulation.<sup>21,28,29</sup> In the lung and mLN, primary (1M)  $T_{RM}$  generated by one influenza infection wane in number



with time, whereas quaternary (4M)  $T_{RM}$  that have responded to four distinct influenza infections exhibit enhanced longevity and protective capacity in these respiratory tissues.<sup>28,29</sup> 4M  $T_{CIRCM}$  isolated from the spleen also begin to transcriptionally resemble  $T_{RM}$  populations.<sup>29</sup> Beyond influenza-focused studies, investigations of multiply stimulated CD8 $^{+}$  T cells out to 51M generations have been conducted with peripheral vesicular stomatitis virus (VSV) infection.<sup>32</sup> These investigations have revealed that the expansive, proliferative, and protective capacities of virus-specific  $T_{CIRCM}$  following spaced, repetitive antigen stimulations are preserved despite increased inhibitory receptor expression (i.e., PD-1 and TIM-3).<sup>32</sup> However, these functions may exhibit sensitivity to elapsed time since the last antigen stimulation and the indicated pathogen selected for rechallenge.<sup>21,23,26</sup> Finally, memory CD8 $^{+}$  T cell tolerance for self and tumor antigens can be overcome with repetitive stimulation, suggesting an impact beyond pathogen-specific responses.<sup>30</sup> Collectively, these previously published data underscore the profound impact of repetitive antigen exposure on the composite memory CD8 $^{+}$  T cell pool. However, further investigations are needed to understand how memory T cell populations are shaped in discrete tissue environments that may not be directly infected (i.e., brain) following repeated peripheral viral infections.

Pathogen-specific brain  $T_{RM}$  are thought to exert protective functions via “sense and alarm” actions that alert the local and peripheral immune system to intracranial infection.<sup>43</sup> Upon rechallenge, peripheral-infection-induced brain  $T_{RM}$  rapidly upregulate cytokines like interferon gamma (IFN $\gamma$ ) and cytolytic molecules such as granzyme B.<sup>13,19,38</sup> This response is thought to activate microglia and recruit peripheral immune cells to infected brain tissue.<sup>10,11,19</sup> Collectively, brain  $T_{RM}$  protect against neurotropic pathogens that would otherwise engender high mortality in an antigen-dependent manner.<sup>13</sup> As viral pathogens with neurotropic potential continue to evolve (i.e., SARS-CoV-2, H5N1 influenza virus), investigating the neuroprotective mechanisms of brain  $T_{RM}$  seeded by one or multiple rounds of previous peripheral viral infection may help unveil composite adaptive responses in this critical tissue site. To date, the ability of repetitively stimulated brain  $T_{RM}$  to mediate neuroprotective outcomes is unknown.

Resolving single vs. repetitively stimulated memory CD8 $^{+}$  T cells in the human brain is challenging, in part due to (1) the lack of definitive biomarkers that identify memory T cells with previous antigen exposures, (2) the diverse and unspecified infection histories of humans, and (3) the invasive nature of brain-based sampling. Therefore, we investigated brain  $T_{RM}$  with single or repetitive antigen stimulation histories in tractable mouse models of peripheral viral infection.

## RESULTS

### Prior antigen stimulation among CD8 $^{+}$ T cells restricts the formation of new brain $T_{RM}$

To address the impact of repetitive antigen exposure on CD8 $^{+}$  brain  $T_{RM}$ , we first identified a mouse model system that enabled the generation of memory CD8 $^{+}$  T cell populations with known numbers of antigen encounters after non-neurotropic influenza A infection. To eliminate variability based on the TCR repertoire, we leveraged our previously published model that utilizes repet-

itive adoptive transfer of naive or  $T_{CIRCM}$  TCR transgenic (TCR-tg) CD8 $^{+}$  T cells into infected hosts.<sup>21,22,24,25,27–29</sup> Initially, naive Thy1.2 C57BL/6 mice were seeded with low numbers ( $10^4$ ) of naive Thy1.1 CD8 $^{+}$  TCR-tg P14 cells recognizing the GP<sub>33–41</sub> epitope of lymphocytic choriomeningitis virus (LCMV) (Figure 1A). These mice were subsequently infected intranasally (I.N.) with recombinant PR8 influenza A virus expressing GP<sub>33–41</sub> (PR8-GP33). At a memory time point >45 days post-infection, 10 $^5$  spleen-derived 1M P14 cells were transferred into new, naive congenic recipients that were subsequently infected with PR8-GP33. The higher number of P14  $T_{CIRCM}$  transferred normalizes memory P14 numbers in the periphery following infection with those obtained from naive P14 progenitors.<sup>21,27–29</sup> Adoptive transfers and viral infections were repeated until mice harboring 1M and 4M P14 cells could be compared. Critically, this strategy (1) achieves similar frequencies of 1M and 4M P14  $T_{CIRCM}$ , enabling the study of tissue-isolated outcomes, (2) unambiguously demarcates memory T cells with specified antigen exposure histories, and (3) abrogates neutralizing antibody-mediated protection against surface viral antigens that offer limited heterosubtypic immunity against mutation-prone and antigenically plastic viruses such as influenza.<sup>44</sup> Consequently, the ability to study memory CD8 $^{+}$  T cells with specificity for conserved, internal viral proteins after repetitive influenza infection is optimized in this experimental approach.

We first asked whether repetitively stimulated memory CD8 $^{+}$  T cells could be identified in the spleen and brain. Intravascular (IV) exclusion was performed prior to tissue harvest by intravenously injecting a fluorophore-conjugated anti-CD45 antibody to distinguish immune cells in the brain vasculature (IV+) from immune cells localized within the brain tissue (IV–).<sup>45</sup> As expected from prior work, the frequencies and numbers of 1M and 4M P14 cells in the spleen were similar after influenza infection, suggesting a similar generation of  $T_{CIRCM}$  (Figures 1B–1D and S1).<sup>28,29</sup> However, within the IV– fraction of the brain, the proportion of 4M P14 cells was substantially reduced compared to 1M counterparts, with a ~2.6-fold reduction in total numbers (Figures 1B–1D). We next wished to determine the identity of these 1M and 4M P14 cells as  $T_{CIRCM}$  or  $T_{RM}$ . Body-surveilling  $T_{CIRCM}$  composed of T central memory cells ( $T_{CM}$ ) and T effector memory cells ( $T_{EM}$ ), as well as organ-embedded  $T_{RM}$ , can be broadly discerned via differential expression of CD62L, a lymph node homing marker, and CD69, a residency marker at homeostatic time points.<sup>33,37</sup> Within the spleen, we observed an expected decline in  $T_{CM}$  identity among 4M P14 cells compared to 1M P14 cells, reflecting previously published outcomes among repetitively stimulated  $T_{CIRCM}$  (Figures 1E and 1F).<sup>21,29</sup> However, within the IV– brain, a similar proportion of 1M and 4M P14 cells upregulated CD69, consistent with a previously identified brain  $T_{RM}$  phenotype (Figures 1G and 1H).<sup>6</sup> Furthermore, the expression of residency-associated markers CXCR6 and CD49a also did not vary among 1M and 4M P14 brain  $T_{RM}$  (Figure S2). Finally, the number and phenotypes of non-P14 endogenous  $T_{CIRCM}$  and  $T_{RM}$  were equivalent in hosts harboring either 1M or 4M P14 cells, verifying that the differences in antigen exposure history underlie the observed differences in brain P14 cells (Figure S3). Together, these results suggest that prior repetitive antigen stimulation history may specifically restrict the formation of new brain  $T_{RM}$  from peripheral  $T_{CIRCM}$ .

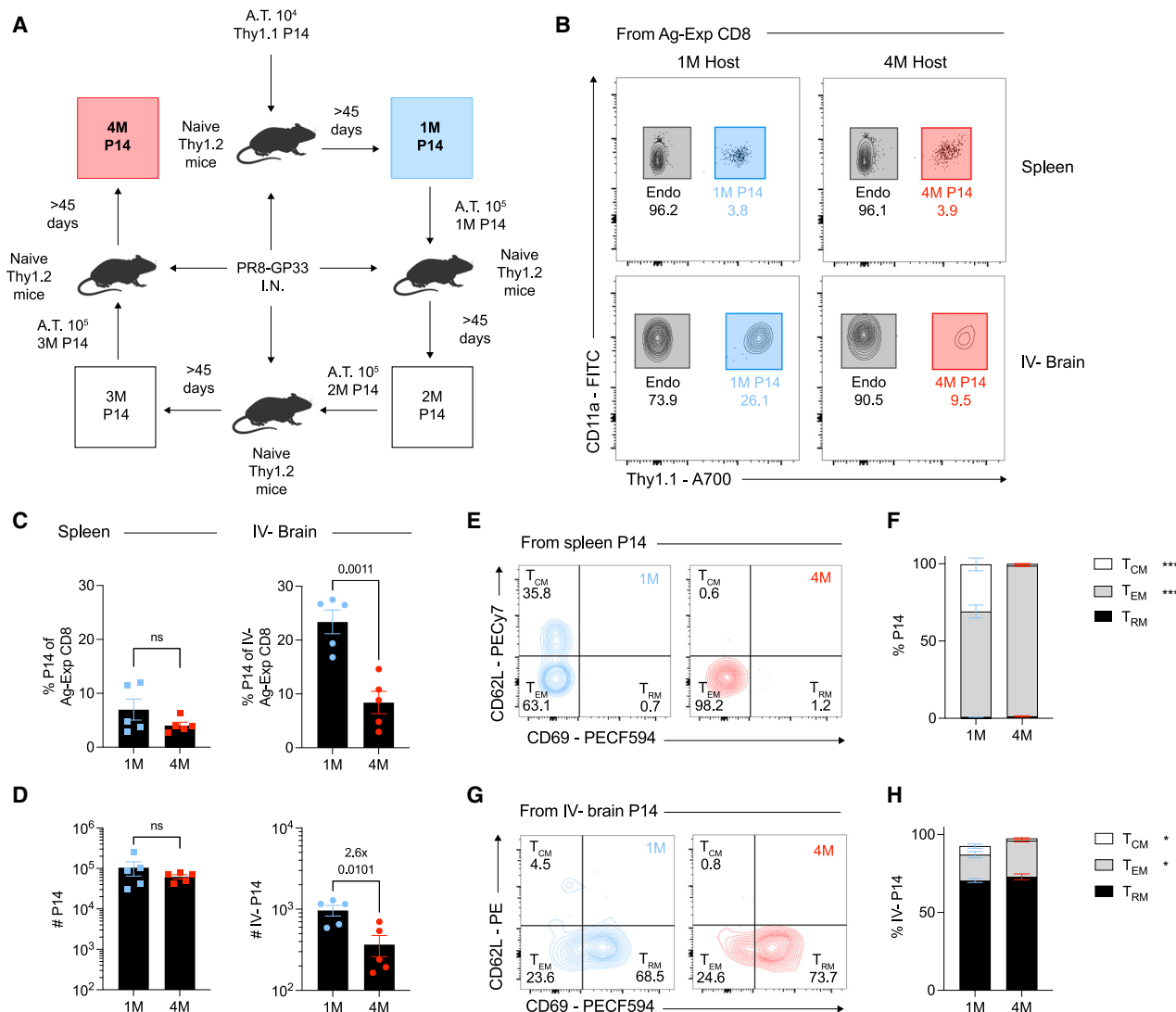


**Figure 1. The representation of influenza-specific memory CD8<sup>+</sup> T cells in the brain is reduced following repetitive antigen stimulation**

(A) Experimental design of repetitively stimulated memory CD8<sup>+</sup> T cell generation. Sequential Thy1.1 P14 adoptive transfer (A.T.) and intranasal (I.N.) infection with PR8-GP33 were employed to generate primary (1M, blue), secondary (2M), tertiary (3M), and quaternary (4M, red) P14 T cells in Thy1.2 C57BL/6 mice. Splenic harvests for P14 A.T. or tissue harvests for cell analysis were performed >45 days following infection.

(B) Representative flow plots of CD11a<sup>hi</sup> antigen-experienced (Ag-Exp) memory CD8<sup>+</sup> T cells isolated from the spleens and intravascular stain-negative (IV-) brains of 1M and 4M P14 cell-bearing mice.

(C and D) Proportion (C) and number (D) of splenic and brain-derived 1M/4M P14 cells.

(E and F) Representative flow plots (E) and proportions (F) of splenic 1M and 4M P14 cells to delineate cellular identity as T central memory (T<sub>CM</sub>: CD62L<sup>+</sup>, CD69<sup>-</sup>), T effector memory (T<sub>EM</sub>: CD62L<sup>-</sup>, CD69<sup>-</sup>), or tissue-resident memory (T<sub>RM</sub>: CD62L<sup>-</sup>, CD69<sup>+</sup>).

(G and H) Same as (E) and (F) but for IV- brain-derived P14 cells.

Experiments in (A)-(H) show data from 1 of 2 independent experiments with  $n = 4-5$  mice per group in each experiment. Statistical significance was determined by Student's t test using GraphPad Prism. Graphs show the mean  $\pm$  SEM, with each symbol representing one mouse. Individual p values are noted on the respective graphs or are summarized as follows: \* $p < 0.05$ , \*\* $p < 0.01$ , \*\*\* $p < 0.001$ , and \*\*\*\* $p < 0.0001$ . Graphical illustrations were created using BioRender (<https://biorender.com>).

### The reduced presence of repetitively stimulated brain T<sub>RM</sub> is conserved across peripheral viral infections and time

We have previously shown that several peripheral viral infections in mice can generate CD8<sup>+</sup> brain T<sub>RM</sub>.<sup>13</sup> Therefore, we addressed whether a peripheral viral infection other than influenza

A virus would impart similar outcomes among 1M and 4M P14 cells in the brain. To accomplish this, we infected mice intraperitoneally (I.P.) with LCMV strain Armstrong, which causes an acute systemic infection with minimal CNS involvement to generate heterozygous 3M Thy1.1/2 P14 memory CD8<sup>+</sup> T cells as in Figure 1A.<sup>46,47</sup> Subsequently, Thy1.2 recipient

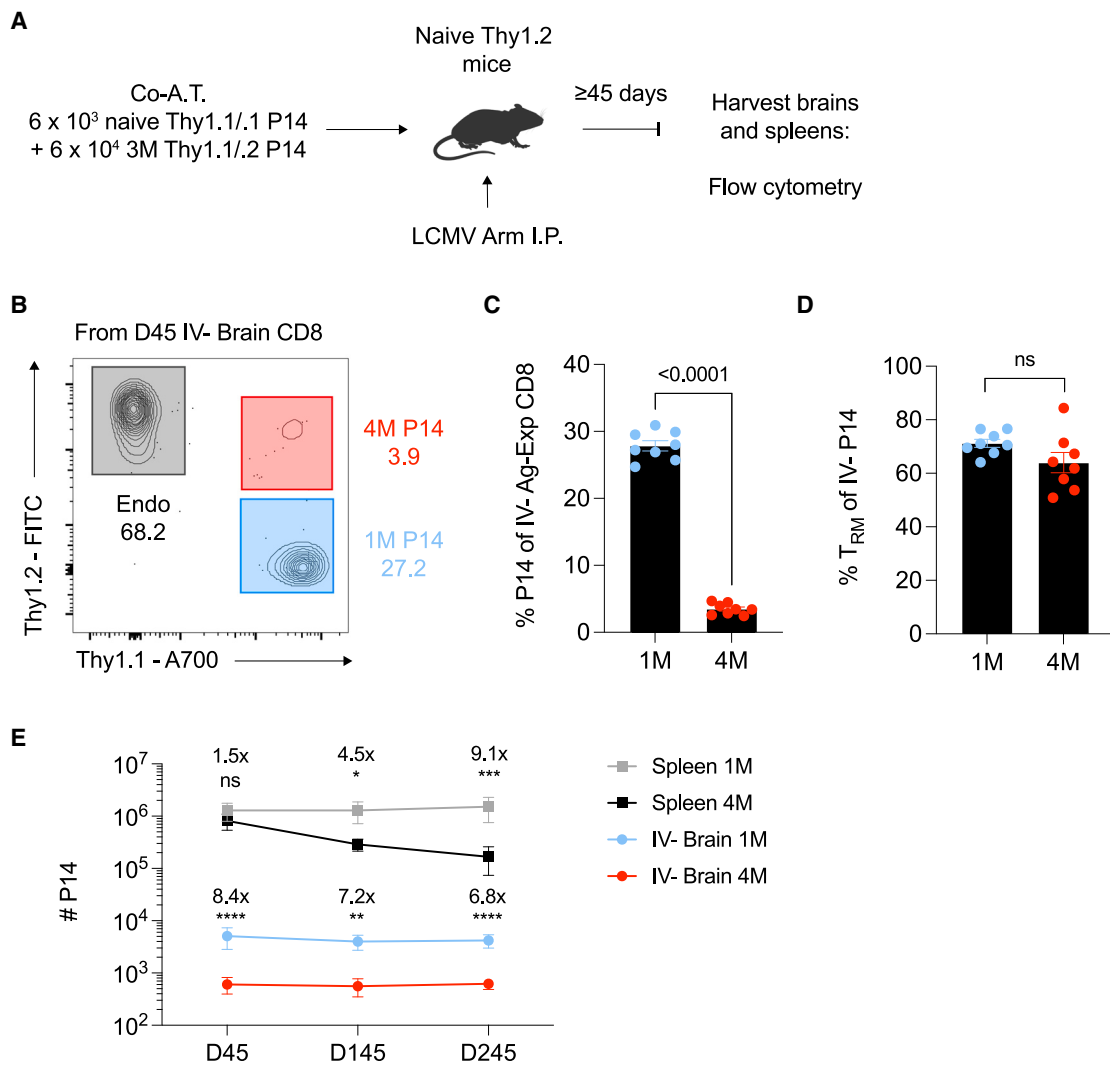


**Figure 2. The reduced representation of repetitively stimulated brain T<sub>RM</sub> is conserved across viral infection models and memory time points**

(A) Experimental design of repetitively stimulated memory CD8<sup>+</sup> T cell generation using co-adoptive transfer (Co-A.T.) of Thy1.1/1 naive P14 or Thy1.1/2 3M P14 cells into the same naive Thy1.2/2 murine host. Mice were infected with lymphocytic choriomeningitis virus (LCMV) strain Armstrong intraperitoneally (I.P.) as a comparative infection approach 1 day following co-A.T. and were analyzed ≥45 days after infection.

(B) Representative flow plot of IV- Ag-Exp CD8<sup>+</sup> T cells isolated from the brains of co-A.T. hosts, comprised of endogenous memory (endo), 1M P14, and 4M P14 populations at day 45.

(C) Proportion of IV- brain CD8<sup>+</sup> T cells that are either 1M or 4M P14.

(D) Frequency of CD69<sup>+</sup> T<sub>RM</sub> among 1M and 4M P14 cells in the IV- brain.

(E) Number of 1M or 4M P14 cells isolated from the spleen or IV- brain tissue of LCMV-experienced mice at day 45, 145, or 245 post-infection. Numeric fold changes and significance are noted between 1M and 4M P14 cells isolated from the matched tissue type at the same time point with co-adoptively transferred hosts.

Experiments in (A)-(E) show data from 2 of 2 independent experiments with  $n = 4-8$  mice combined at each time point. Statistical significance was determined by Student's t test using GraphPad Prism at each time point. Graphs show the mean ± SEM with each symbol representing one mouse (C and D) or mean ± SD (E), with each symbol representing one mouse. Individual p values are noted on the respective graphs or are summarized as follows: \* $p < 0.05$ , \*\* $p < 0.01$ , \*\*\* $p < 0.001$ , and \*\*\*\* $p < 0.0001$ . Graphical illustrations were created using BioRender (<https://biorender.com>).

mice were co-adoptively transferred with both naive Thy1.1/1 P14 cells and 3M Thy1.1/2 P14 cells to allow for the evaluation of 1M and 4M P14 cells in the same host after LCMV infection (Figure 2A). Like the results from PR8-GP33 infection, the IV- brain harbored a markedly greater proportion of 1M P14 T<sub>RM</sub> compared to 4M P14 T<sub>RM</sub> 45 days following peripheral LCMV

infection (Figures 2B–2D). These data demonstrated that the reduced presence of 4M compared to 1M T<sub>RM</sub> in the brain is conserved across at least two viral model systems.

The maintenance of 1M and 4M memory CD8<sup>+</sup> T cells is highly dependent on tissue localization. 4M T<sub>CIRCM</sub> in the spleen slowly wane in number across time without restimulation, unlike 1M

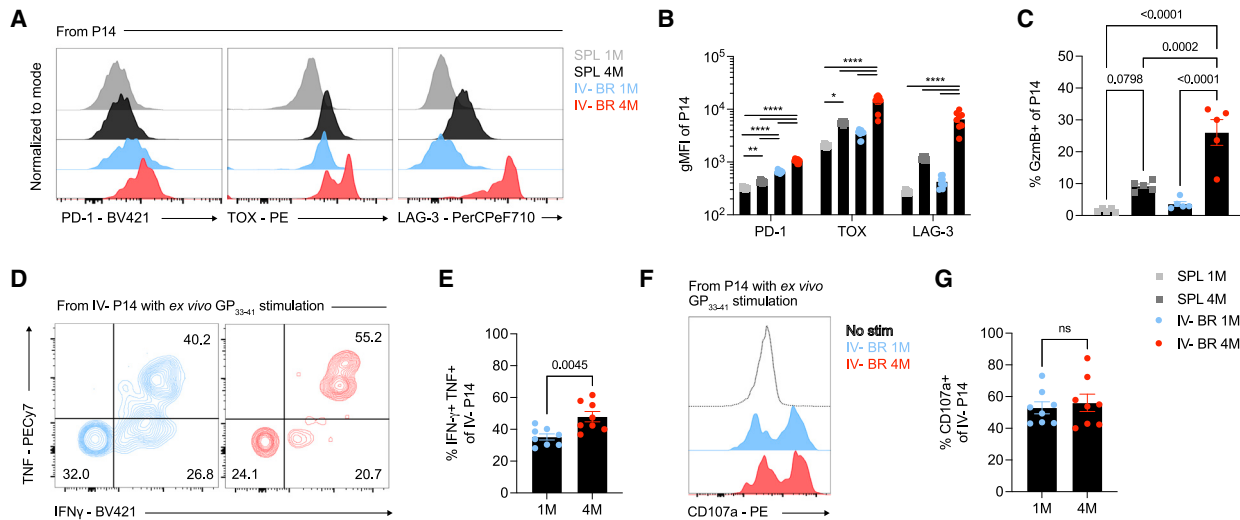


**Figure 3. Repetitive peripheral antigen stimulation enhances inhibitory receptor expression without functional attrition among brain  $T_{RM}$**   
 (A and B) Representative histograms (A) and geometric mean fluorescent intensity (gMFI) (B) of PD-1, TOX, and LAG-3 expression, respectively, among 1M and 4M P14 cells from the spleen (SPL) or IV – brain (IV – BR) of co-A.T. LCMV-experienced hosts at day 45.  
 (C) Proportion of granzyme B (GzmB+) 1M and 4M P14 cells without ex vivo stimulation.  
 (D) Representative flow plot of IFN $\gamma$  and TNF expression among 1M and 4M P14 cells from the IV – brain of co-A.T. LCMV-experienced hosts following 5-h ex vivo incubation with 200 nM GP<sub>33–41</sub> peptide.  
 (E) Proportion of IFN $\gamma$ + TNF+ -expressing 1M and 4M P14 cells following peptide stimulation.  
 (F and G) Representative histogram (F) and proportion (G) of CD107a+ P14 cells following ex vivo GP<sub>33–41</sub> peptide stimulation.  
 Experiments in (A)–(G) show data from 1 of 2 independent experiments with  $n = 5$ –8 mice per group in each experiment. Statistical significance was determined by one-way ANOVA with Tukey's multiple comparisons post-test or Student's t test using GraphPad Prism. Graphs show the mean  $\pm$  SEM, with each symbol representing one mouse. Individual  $p$  values are noted on the respective graphs or are summarized as follows: \* $p < 0.05$ , \*\* $p < 0.01$ , \*\*\* $p < 0.001$ , and \*\*\*\* $p < 0.0001$ .

counterparts.<sup>21</sup> In contrast, within the lung and mLN, 4M  $T_{RM}$  persist longer than 1M cells.<sup>28,29</sup> To query the impact of antigen stimulation history on brain  $T_{RM}$ , we compared the numbers of 1M and 4M P14 cells at days 45, 145, and 245 post-LCMV infection in the spleen and IV – brain. We first noted an expected numeric decline in 4M P14  $T_{CIRCM}$  in the spleen at late time points, while 1M P14  $T_{CIRCM}$  numbers remained stable (Figure 2E).<sup>21</sup> However, in the IV – brain, the elevated ratio of 1M:4M P14  $T_{RM}$  was stably maintained across all tested time points. Together, our data suggest that the reduced representation of 4M  $T_{RM}$  in the brain compared to 1M counterparts is established at early memory time points following peripheral infection and is durably maintained across time.

#### Repetitive stimulation enhances inhibitory receptor expression without attrition in function

Repetitive antigen stimulation history and tissue localization can independently shape the phenotype and function of memory T cells. PD-1 expression is elevated in  $T_{RM}$  from several non-lymphoid tissues, including from the murine and human brain, compared to  $T_{CIRCM}$ .<sup>6,13,19,38,48,49</sup> In parallel, repetitive antigen stimulation elevates PD-1, LAG-3, TIM-3, and TOX expression among  $T_{CIRCM}$ .<sup>21,23,29,32</sup> Accordingly, following peripheral LCMV infection in co-adoptively transferred hosts, we analyzed inhibitory receptor expression among 1M and 4M P14 cells derived from the spleen or IV – brain. Among all memory popula-

tions queried, 4M brain P14 cells exhibited the highest expression of PD-1, LAG-3, and TOX (Figures 3A and 3B). These outcomes were similarly shared by 4M brain P14 cells generated by PR8-GP33 peripheral infection, suggesting a conserved phenotype across viral infection models (Figures S4A and S4B). These data suggested that the collective impact of repetitive antigen stimulation and brain localization poised 4M brain  $T_{RM}$  to exhibit pronounced inhibitory receptor expression.

Although elevated inhibitory receptors can demarcate exhausted T cells during chronic viral infection, the expression of PD-1, LAG-3, and/or TOX does not necessarily equate to reduced functionality among primary or repetitively stimulated memory T cells generated by known acute viral infections.<sup>32,50</sup> To contextualize the functional significance of elevated inhibitory receptor expression among 4M P14 cells in the brain, we performed ex vivo studies to assess cytolytic- and cytokine-producing potential. It was first noted that 4M P14  $T_{RM}$  exhibited enhanced expression of granzyme B directly ex vivo, suggestive of a poised cytolytic state compared to 1M  $T_{RM}$  and  $T_{CIRCM}$  populations (Figure 3C). Granzyme B expression was also enhanced among 4M brain  $T_{RM}$  generated by PR8-GP33 peripheral infection (Figures S4C and S4D). Upon ex vivo stimulation with the GP<sub>33–41</sub> peptide, the proportion of IFN $\gamma$ -producing cells was similar between 1M and 4M P14 brain  $T_{RM}$ , whereas 4M cells exhibited a modestly elevated ability to co-express tumor necrosis factor (TNF) (Figures 3D and 3E). Finally, the frequency of CD107a+ cells, indicative of degranulation following peptide

stimulation, was similar between 1M and 4M T<sub>RM</sub> (Figures 3F and 3G). Together, these results suggest that repetitive antigen stimulation history and tissue localization converge to increase inhibitory receptor expression among 4M brain T<sub>RM</sub>. However, the elevated expression of these markers does not necessarily denote reduced functionality among 4M T<sub>RM</sub> in the brain.

### Repetitively stimulated brain T<sub>RM</sub> are proportionally enriched in the choroid plexus

Previous studies of T<sub>RM</sub> in non-lymphoid organs (i.e., lung, skin, intestine) have revealed that memory T cells exhibit numeric, phenotypic, transcriptional, and epigenetic variation based on anatomical niches within an organ.<sup>51–57</sup> However, such localization studies have not been rigorously applied to the study of repetitively stimulated memory CD8<sup>+</sup> T cells or brain T<sub>RM</sub>. To distinguish potential regions of 1M or 4M enrichment within the brain, we devised a physical dissection approach to separately assess the parenchyma, cerebrospinal fluid (CSF), and choroid plexus (Figure 4A). Of importance, unlike the blood-brain-barrier-restricted parenchyma and blood-CSF-barrier-restricted CSF, the choroid plexus exhibits a fenestrated endothelium that interfaces with the brain vasculature. At days 60 and 245 post-LCMV infection in co-adoptively transferred hosts, the brain region with the highest frequency of 4M P14 brain T<sub>RM</sub> was the choroid plexus (Figures 4B–4D). Parenchymal 1M and 4M P14 T<sub>RM</sub> largely remained stable across time. In contrast, choroid plexus 1M T<sub>RM</sub> diminished in number, reflecting a potential epithelial-poised outcome that is also shared by 1M T<sub>RM</sub> in the lung (Figures 4E and 4F).<sup>28,58</sup> Altogether, these data suggest that diverse brain niches are seeded with T<sub>RM</sub> of varying antigen stimulation histories and that repetitively stimulated brain T<sub>RM</sub> may be more highly represented in the choroid plexus.

### Brain memory CD8<sup>+</sup> T cells can be visualized in the choroid plexus, neurogenic niches, and parenchymal white matter

T cells have been identified in specific brain compartments of humans experiencing neurological health or disease. However, the expanse of brain T<sub>RM</sub> with varying antigen stimulation histories across solid brain compartments (i.e., choroid plexus and parenchyma) remains unknown (Figure 5A). To address this, we first examined 1M and 4M P14 cells from the fourth ventricle choroid plexus of PR8-GP33 and LCMV-experienced hosts (Figure 5B). We observed a diffuse distribution of both 1M and 4M P14 cells across this barrier tissue. We then investigated parenchymal regions of interest, such as neurogenic niches and white matter, that have previously been shown to harbor T<sub>RM</sub> in healthy human brain specimens.<sup>49,59</sup> Neurogenic niches, such as the dentate gyrus of the hippocampus and subventricular zone, serve as rare, regenerative regions of brain that harbor neural stem cells. In contrast, white matter regions relay neural signals via dense projections of myelinated axons in the brain. In 1M and 4M P14 cell-bearing hosts, we observed the widespread presence of P14 cells in both neurogenic niches and white matter regions (Figures 5C and 5D). Across choroid plexus and parenchymal brain regions, 1M P14 cells were more highly represented in LCMV-experienced hosts, congruent with our flow cytometric results (Figure 5E). Together, these results verify a widespread

distribution of 1M and 4M T<sub>RM</sub> across the brain and suggest that virus-specific T<sub>RM</sub> are poised at both brain border and parenchymal sites.

### 4M P14 T<sub>RM</sub> provide protection similar to that of 1M P14 cells against intracranial infection and promote enhanced recruitment of peripheral T cells

Peripherally induced 1M brain T<sub>RM</sub> in mice exhibit potent abilities to reduce morbidity and mortality during antigen-matched, intracranial infections.<sup>13</sup> The potential protective contribution of 4M brain T<sub>RM</sub> to rechallenge contexts remains unknown. Furthermore, the neuroprotective mechanisms of 1M and/or 4M brain T<sub>RM</sub> during *in vivo* intracranial infections are largely unspecified. Therefore, we first asked whether 4M brain T<sub>RM</sub> could provide protection against intracranial infection despite numeric scarcity and, secondarily, asked how 1M vs. 4M brain T<sub>RM</sub>-initiated recall responses differed. To accomplish this, we leveraged our previously published model of *in vivo* intracranial rechallenge.<sup>13</sup> Briefly, LCMV-naïve mice or LCMV-experienced mice harboring 1M or 4M P14 cells were employed (Figure 6A). At a memory time point, LCMV-experienced mice were depleted of P14 T<sub>CIRCM</sub> utilizing a low-dose anti-Thy1.1 (a-Thy1.1) antibody that preserves P14 brain T<sub>RM</sub>, enabling the isolation of T<sub>RM</sub>-based action only.<sup>13</sup> Once the successful depletion of P14 T<sub>CIRCM</sub> was confirmed, mice were intracranially (I.C.) challenged with attenuated, recombinant *Listeria monocytogenes* expressing GP<sub>33–41</sub> (rLM-GP33), where the GP<sub>33–41</sub> epitope recognized by P14 cells is the only common antigen between infections (Figures 6B and 6C). Notably, 3 days post-rLM-GP33 challenge, mice harboring 1M or 4M P14 brain T<sub>RM</sub> exhibited similarly reduced bacterial burdens compared to LCMV-naïve hosts (Figure 6D). This outcome was accomplished despite the stark numeric discrepancy between 1M and 4M P14 T<sub>RM</sub> during rechallenge (Figure 6E). We validated that these outcomes were specific to 4M brain T<sub>RM</sub>-based action by treating mice with FTY720 to diminish lymphocyte recruitment (Figure S5A). Similar to our previously published findings of 1M brain T<sub>RM</sub>-sufficient protection, FTY720 treatment did not perturb protective outcomes by 4M brain T<sub>RM</sub> (Figure S5B).<sup>13</sup> Finally, we verified that 1M and 4M brain T<sub>RM</sub> could only wield antigen-specific protection, as intracranial infection of 1M or 4M hosts with rLM expressing the *Plasmodium*-derived peptide GAP50<sub>40–48</sub> did not confer protection compared to naïve control mice (Figure S5C). These data indicate that like antigen-specific 1M brain T<sub>RM</sub>, 4M T<sub>RM</sub> are also capable of wielding neuroprotective outcomes.

Prior studies have shown that the protective capacity of primary and repetitively stimulated CD8<sup>+</sup> T cells manifest in pathogen-specific abilities to control challenge infection.<sup>23</sup> Thus, we next asked whether 4M T<sub>RM</sub> elicit differential recall responses from 1M T<sub>RM</sub>. We first broadly performed immunophenotyping in rechallenged hosts (Figure S6). Here, we observed that hosts with 4M P14 T<sub>RM</sub> exhibited increased numbers of CD4<sup>+</sup> and CD8<sup>+</sup> T cells in the infected brain after intracranial challenge relative to naïve and 1M P14 hosts (Figures 6F–6H). We also observed greater CD8<sup>+</sup> T cell presence in brain border sites like the choroid plexus, where peripheral T cells could be recruited from the blood (Figure 6I). Unlike T cells, microglia numbers were stable between all groups, and only modest

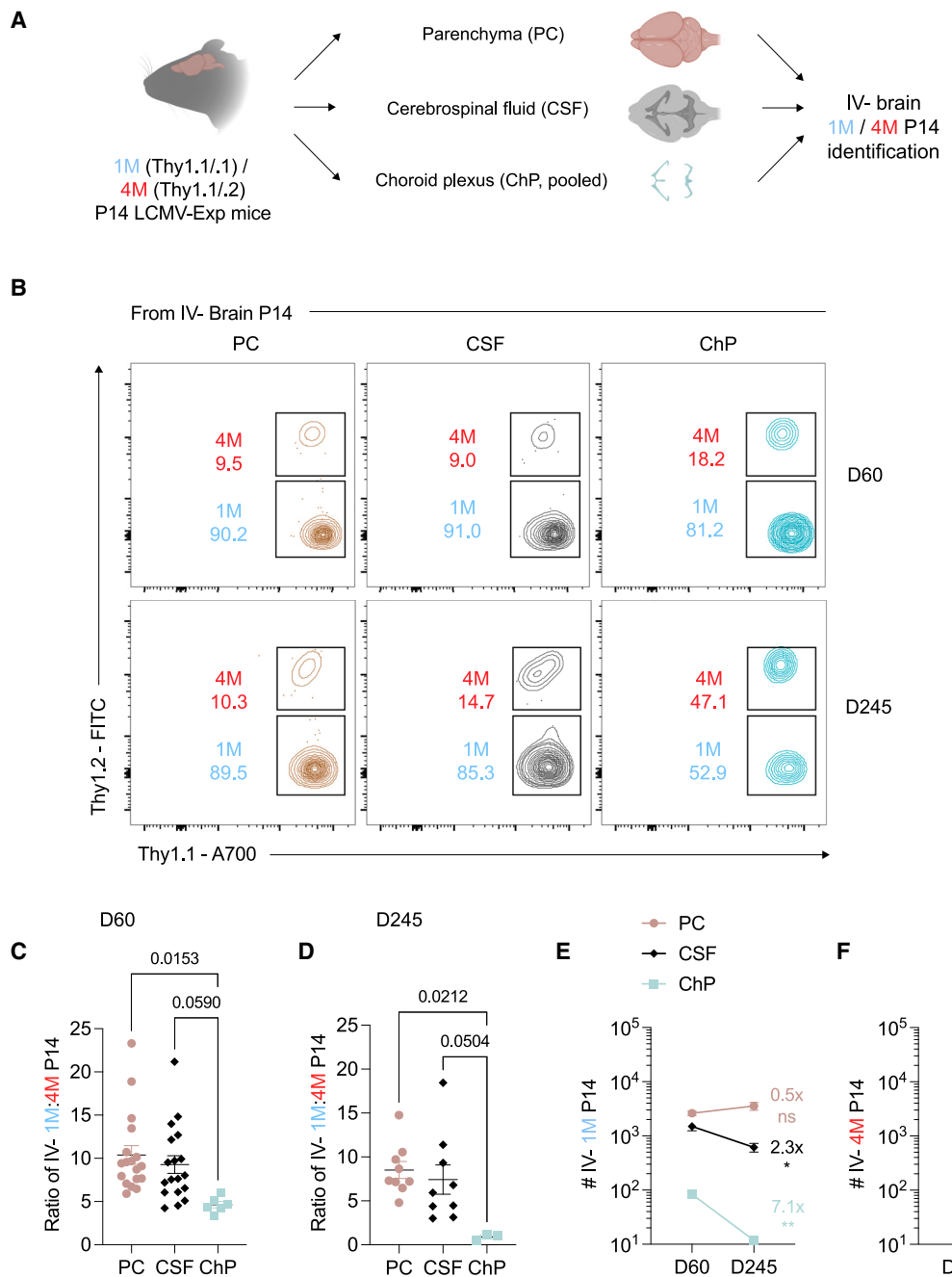


**Figure 4. The representation of primary and repetitively stimulated memory CD8<sup>+</sup> T cells differs by brain compartment**

(A) Illustration demonstrating isolation of parenchyma (PC), cerebrospinal fluid (CSF), and choroid plexus (ChP; pooled from lateral, third, and fourth ventricles of  $n = 3$  mice) from the brain tissue of co-A.T. LCMV-experienced mice. 1M and 4M P14 cells from the IV- brain were isolated at day 60 or 245 following LCMV infection.

(B) Representative flow plots demonstrating the distribution of 1M/4M cells among P14 cells in each IV- brain compartment at days 60 and 245 post-LCMV infection.

(C and D) Ratio of 1M:4M P14 cells in the IV- PC, CSF, and ChP at days (C) 60 and (D) 245.

(E and F) Number of (E) 1M and (F) 4M P14 in each brain compartment across time points.

Experiments in (A)-(F) show data from 2 of 2 independent experiments with  $n = 6-9$  mice per group in each experiment. Statistical significance was determined by one-way ANOVA with Tukey's multiple comparisons post-test or Student's t test using GraphPad Prism. Graphs show the mean  $\pm$  SEM, with each symbol representing one mouse (C and D). Graphs show the mean  $\pm$  SEM (E and F). Individual  $p$  values are noted on the respective graphs or are summarized as follows:

\* $p < 0.05$ , \*\* $p < 0.01$ , \*\*\* $p < 0.001$ , and \*\*\*\* $p < 0.0001$ . Graphical illustrations were created using BioRender (<https://biorender.com>).

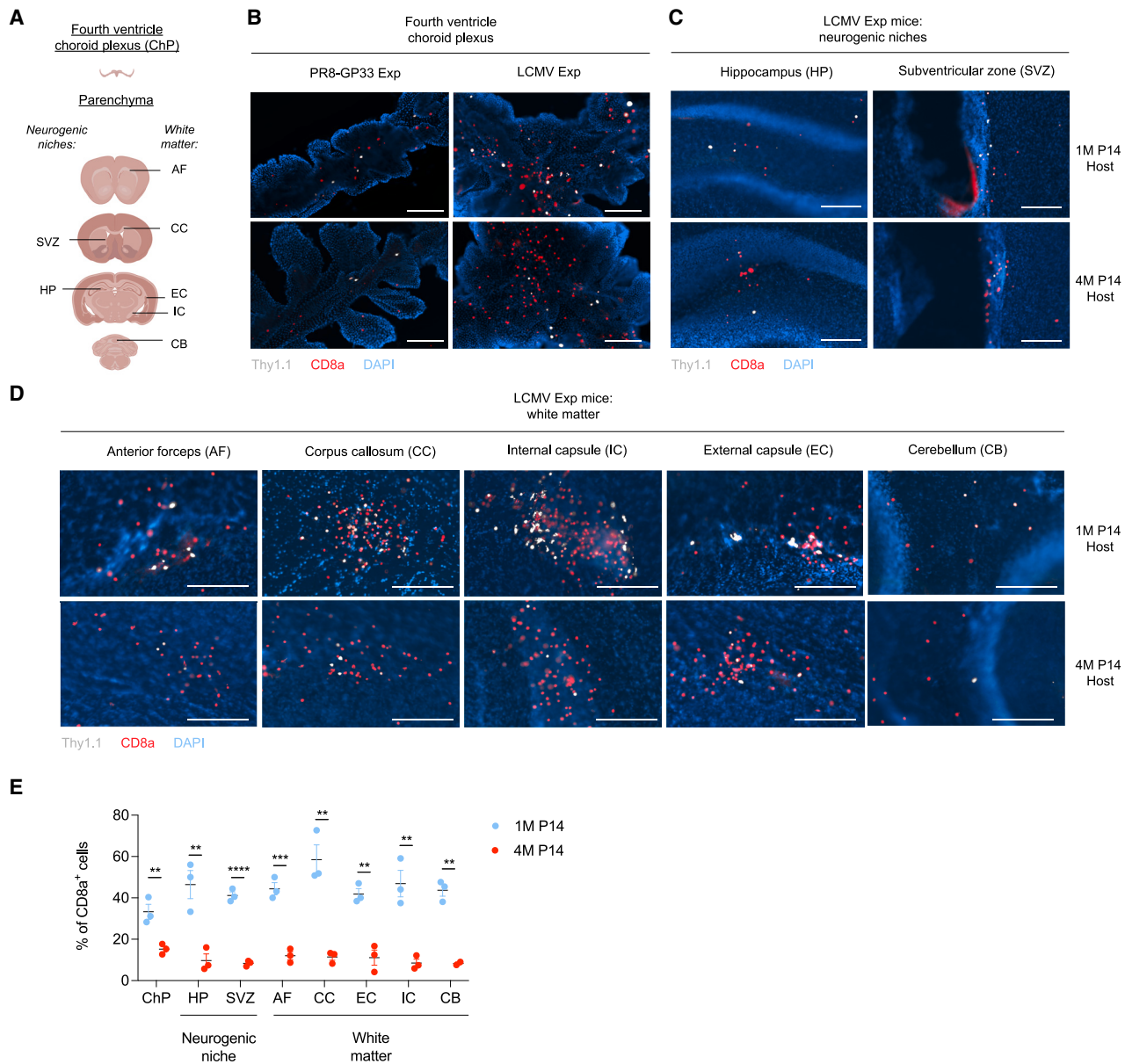


**Figure 5. 1M and 4M P14 brain T<sub>RM</sub> can be visualized in solid brain compartments**

(A) Illustration demonstrating isolation of choroid plexus and parenchymal brain (neurogenic niches and white matter regions) via serial sectioning for staining.

(B) Representative immunofluorescent images of Thy1.1<sup>+</sup> P14 cells (gray), CD8 $\alpha$ <sup>+</sup> T cells (red), and DAPI<sup>+</sup> nucleated cells (blue) across the fourth ventricle choroid plexus of PR8-GP33 or LCMV-experienced (Exp) hosts bearing 1M or 4M P14 cells >45 days after infection.

(C) Representative immunofluorescent images of Thy1.1<sup>+</sup> P14 cells (gray), CD8 $\alpha$ <sup>+</sup> T cells (red), and nucleated cells (blue) across neurogenic niches (i.e., the hippocampus [HP] and subventricular zone [SVZ]) in LCMV-Exp hosts bearing 1M or 4M P14 cells >45 days after infection.

(D) Same as in (B) but for white matter regions including the anterior forceps (AF), corpus callosum (CC), internal capsule (IC), external capsule (EC), and cerebellum (CB).

(E) Proportion of 1M or 4M P14 cells among CD8 $\alpha$ <sup>+</sup> cells across brain regions tested.

Experiments in (A)–(C) show one representative image from  $n = 3$  replicate mice at every brain region. Statistical significance was determined by Student's t test using GraphPad Prism. Graphs show the mean  $\pm$  SEM, with each symbol representing one mouse. Individual  $p$  values are summarized as follows: \* $p < 0.05$ , \*\* $p < 0.01$ , \*\*\* $p < 0.001$ , and \*\*\*\* $p < 0.0001$ . Scale bar: 200  $\mu$ m. Graphical illustrations were created using BioRender (<https://biorender.com>).

reductions in recruited monocytes, neutrophils, and dendritic cells were observed between LCMV-naive hosts and P14 T<sub>RM</sub>-bearing hosts (Figures S7A–S7D). Altogether, these obser-

vations suggest that on a per-cell basis, 4M brain T<sub>RM</sub> are more potent in recruiting peripheral T cells to the brain compared to 1M T<sub>RM</sub>.

We next asked how primary and repetitively stimulated  $T_{RM}$  could modify the local brain environment to facilitate peripheral T cell entry following intracranial infection. Previous work indicates that brain endothelial cells upregulate major histocompatibility complex (MHC) class I and II expression during infectious and inflammatory neuropathologies.<sup>60–63</sup> Furthermore, endothelial MHC class I expression is necessary for the maximal infiltration of effector and memory T cell subsets into non-lymphoid organs following tissue-based infection.<sup>60,64</sup> As such, we investigated whether brain  $T_{RM}$  activation could influence MHC class I or II expression on the brain endothelium as a potential mechanism to enhance T cell recruitment. Here, we observed that CD31<sup>hi</sup>, CD45<sup>−</sup> brain endothelial cells exhibited enhanced expression of MHC class I and II when 1M or 4M brain  $T_{RM}$  were present during rechallenge (Figure 6J–6M). This work suggests that the enhanced recruitment of peripheral T cells in mice with primary and repetitively stimulated brain  $T_{RM}$  coincides with brain endothelial modifications during intracranial infectious challenge.

## DISCUSSION

Here, we have illuminated the numeric, phenotypic, functional, spatial, and protective capacities of CD8<sup>+</sup> brain  $T_{RM}$  with single or repetitive antigen exposure histories. By pairing serial adoptive transfers with two comparative peripheral viral infection models in mice, we have unveiled diversity among brain  $T_{RM}$  that is driven by repeated viral infection. Collectively, these data argue against a monolithic  $T_{RM}$  compartment driven by single infections and point to an investigational need to understand the contribution of repetitively stimulated memory T cells to brain health and disease.

While ubiquitous viral infections such as SARS-CoV-2 and influenza virus are experienced repetitively across the human lifespan, few studies investigate the immunological aftermath of recurring infection. Repeated peripheral viral infection of a single host has the capacity to elicit disparate  $T_{RM}$  responses. Indeed, after successive influenza infections in a single host, lung and mLN  $T_{RM}$  may convert in their antigen stimulation history status (i.e., 1M → 2M → 3M → 4M) due to local viral antigen exposure.<sup>27–29,58</sup> As respiratory-associated  $T_{RM}$  exhibit greater durability with enhanced antigen exposure, this repeated exposure may help to bolster  $T_{RM}$  longevity over time. In contrast, brain  $T_{RM}$  are unlikely to interconvert during non-neurotropic infection due to a lack of available antigen in the brain. Therefore, it is interesting to speculate how peripherally induced brain  $T_{RM}$  of the same TCR specificity may additively accumulate with repeated infection (i.e., 1M+2M+3M+4M). In this scenario, preexisting  $T_{CIRCM}$  could seed new brain  $T_{RM}$  populations without attrition of previously established  $T_{RM}$ . Consequently, it is intriguing to consider whether greater heterogeneity in stimulation history may exist among brain  $T_{RM}$  in humans compared to other antigen-exposed tissues.

The brain is a cellularly and structurally unique tissue. Although studies of repetitively stimulated memory T cells have been primarily isolated from lymphoid organs or respiratory-associated tissues, we have now extracted numeric and phenotypic outcomes in the brain. While repetitively stimulated  $T_{CIRCM}$  and  $T_{RM}$  in peripheral organs are enhanced or similar in representation compared to primary counterparts, our studies suggest a

bias against existing  $T_{CIRCM}$  becoming brain  $T_{RM}$  as efficiently as naive T cells in two peripheral viral model systems. The mechanisms behind this reduced propensity and approaches to overcome this cell-intrinsic obstacle represent exciting areas of future investigation. For example, these studies may help bolster studies of brain-infiltrating chimeric antigen receptor (CAR) T cell therapies, as peripherally derived naive vs. memory T cells may exhibit varying propensities to traffic and form brain  $T_{RM}$  once transduced and infused into patients.<sup>65</sup> Furthermore, we reveal that inhibitory receptor expression is robustly upregulated among virus-specific, 4M brain  $T_{RM}$ . As PD-1 checkpoint blockade has been shown to penetrate CSF, it is interesting to consider how PD-1<sup>hi</sup> repetitively stimulated brain  $T_{RM}$  functionality could become unrestrained, particularly in light of checkpoint-blockade-induced neurological toxicities.<sup>66</sup> Finally, with respect to structure, our investigations suggest that select brain regions, such as the choroid plexus, may be more proportionally enriched for repetitively stimulated brain  $T_{RM}$ . These data bring to light the potential biases or benefits that regional sampling of human brain  $T_{RM}$  may yield.

Repetitively stimulated memory CD8<sup>+</sup> T cells in the brain may be therapeutically leveraged to protect against pathogenic or tumorigenic brain insults.<sup>6</sup> We demonstrate here that despite numeric scarcity, antigen-specific 4M brain  $T_{RM}$  protect hosts against intracranial infection to a degree similar to that of 1M brain  $T_{RM}$ . This outcome also coincided with enhanced recruitment of peripheral T cells. As repetitively infected hosts may simultaneously harbor primary and additive repetitively stimulated memory brain  $T_{RM}$  from subsequent peripheral infections or immunizations, combinatorial action against intracranial infection may be wielded to prevent disease. This work may help contextualize future studies of memory CD8<sup>+</sup> T cell-based immunity in the brain, as emerging strains of SARS-CoV-2 and H5N1 influenza pose worldwide concern for neurotropic conversion. More broadly, this work may inform rational vaccine design and boosting strategies that continue to establish peripherally induced brain  $T_{RM}$  via translationally relevant platforms (i.e., mRNA vaccination). Finally, whether primary or repetitively stimulated brain  $T_{RM}$  protect against brain tumors in antigen-specific or bystander mechanisms is unknown but could underlie disparate responses in viral peptide alarm therapy.<sup>31,38</sup>

The neuropathological roles of repetitively stimulated memory CD8<sup>+</sup> T cells remain an outstanding area of investigation. Peripheral virus or vaccine-induced brain  $T_{RM}$  that exhibit molecular mimicry to CNS antigens are thought to contribute to neurological diseases, such as narcolepsy, neuromyelitis optica, and multiple sclerosis, by targeting orexin neurons and myelin sheaths, respectively.<sup>40,67–70</sup> Whether repeated peripheral infection exacerbates neuroautoimmune disease via increased generation of repetitively stimulated brain  $T_{RM}$  is unclear. Furthermore, it is unknown whether repeated viral infection and concomitant repetitively stimulated  $T_{RM}$  generation could negatively impact brain health in bystander capacities. We demonstrate here that a higher proportion of 4M brain  $T_{RM}$  tonically express granzyme B compared to 1M counterparts. As aging coincides with an increasing likelihood of repeated infection, the contribution of repetitively stimulated brain  $T_{RM}$  to cognitive decline and neurodegenerative disease via bystander cytolytic action stands as a

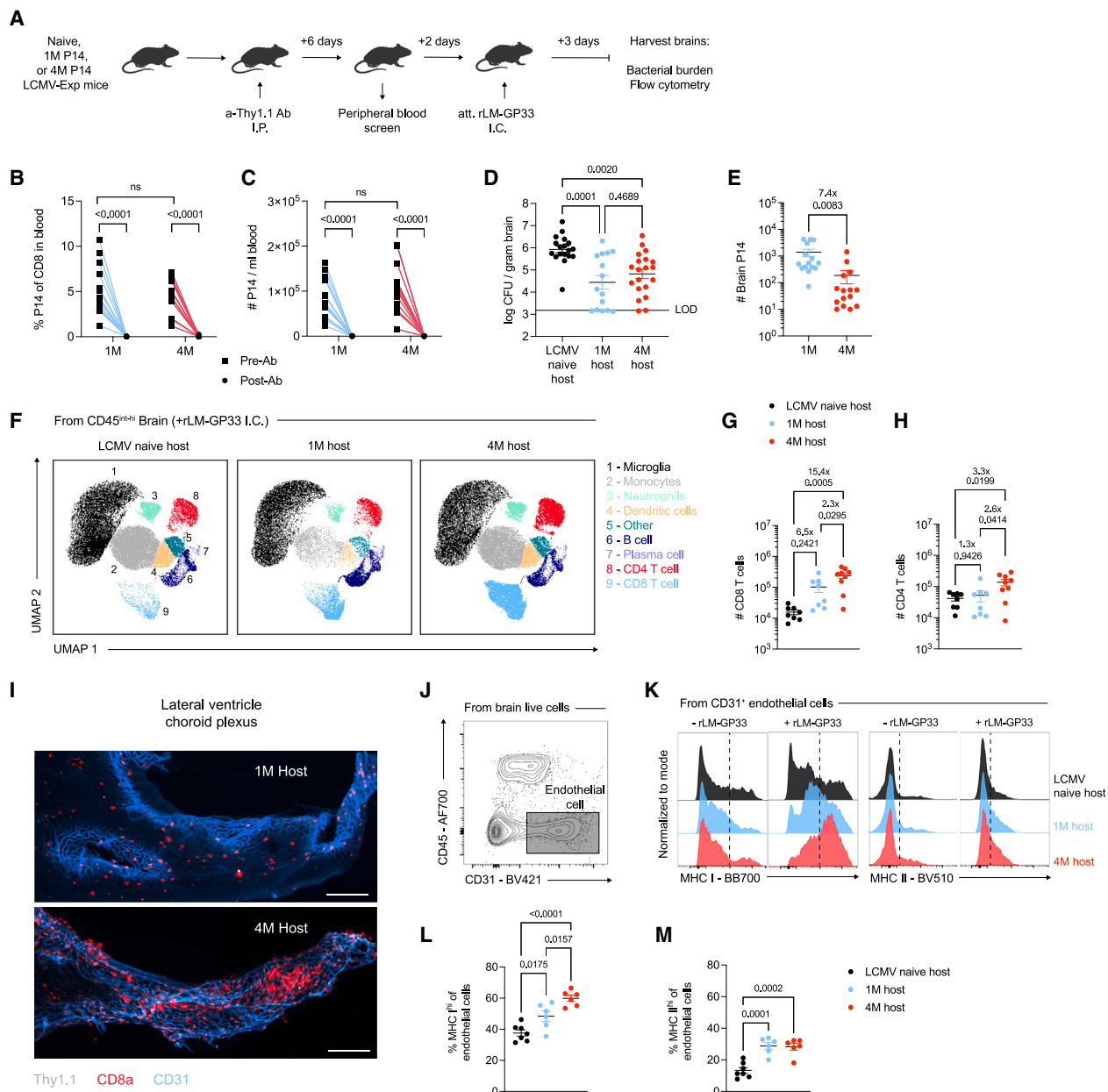


**Figure 6. 1M and 4M brain T<sub>RM</sub> promote enhanced pathogen clearance and differential recall responses following intracranial infection**

(A) Experimental design employing naive or LCMV-experienced hosts bearing 1M or 4M P14 cells >45 days post-infection with peripheral a-Thy1.1-depleting antibody to deplete P14 T<sub>CIRCM</sub>. All mice were intracranially (I.C.) inoculated with 100 colony-forming unit (CFU) attenuated recombinant *Listeria monocytogenes* expressing GP33 (att. rLM-GP33) and analyzed 3 days later.

(B) and (C) Proportion (B) and number (C) of P14 T<sub>CIRCM</sub> in the blood of 1M and 4M hosts before and after a-Thy1.1 antibody depletion.

(D) Log-transformed bacterial CFUs of rLM-GP33 per gram of brain with level of detection (LOD) denoted.

(E) Number of IV- brain P14 cells after intracranial rechallenge.

(F) Uniform manifold approximation and projection (UMAP) plots of 90,000 total downsampled IV- CD45<sup>int-hi</sup> cells derived from the brains of n = 3 pooled mice per group among naive, 1M P14, and 4M P14 hosts after intracranial infection.

(G) and (H) Absolute numbers of (G) CD8<sup>+</sup> T cells and (H) CD4<sup>+</sup> T cells after intracranial infection.

(I) Representative immunofluorescent images of Thy1.1<sup>+</sup> P14 cells (gray), CD8a<sup>+</sup> T cells (red), and CD31<sup>+</sup> endothelial cells (blue) across the choroid plexus of 1M or 4M P14 cell-bearing hosts after intracranial infection.

(J) Representative gating of CD31<sup>+</sup>, CD45<sup>-</sup> brain endothelial cells.

(K-L) Representative histograms (K) and gMFI of MHC class I (L) and MHC class II (M) expression among brain endothelial cells in rLM-GP33 I.C. challenged mice.

(legend continued on next page)

translational relevant question.<sup>10,15,71–76</sup> Importantly, these potential pathological actions can only be rigorously assessed through the intentional generation of repetitively stimulated memory T cells.

In summary, this study supports that brain T<sub>RM</sub> of the same TCR specificity are not a monolithic cell population. While the study of brain T<sub>RM</sub> largely still stems from studies of uninfected mice with low numbers of memory T cells, our work suggests that single and repeated exposure to peripheral viral infection can impart greater diversity to the brain T<sub>RM</sub> pool via the generation of 1M, 2M, 3M, 4M, etc., populations. Consequently, these studies may serve as an example of how repetitive peripheral viral infections can continually reshape the neuroimmune landscape of mammalian hosts. We anticipate that the future generation and study of repetitively stimulated brain T<sub>RM</sub> in mice may help unearth aspects of human post-viral neurological health and disease that cannot be extracted from models of microbial inexperience or single infectious exposure.

### Limitations of the study

Our results address how prior antigen stimulation in the periphery shapes the collective anti-viral brain T<sub>RM</sub> pool. While we surmised that non-neurotropic peripheral infections are more likely to be experienced repetitively, we did not address the impact of repeated neurotropic infection on brain T<sub>RM</sub> populations. During neurotropic infection, the presence of viral-derived antigen or viral-induced damage in the brain may influence T<sub>RM</sub> and/or T<sub>CIRCM</sub> dynamics disparately from our findings with peripheral infection. Our studies also provide a constant inoculum of peripheral virus to generate primary or repetitively stimulated brain T<sub>RM</sub>. In real-world contexts, viral exposures will differ in inoculum dose and severity. In peptide-based stimulation assays to determine functionality, we utilized saturating concentrations of peptide. As the numeric scarcity of 4M brain T<sub>RM</sub> precluded more complete peptide titration studies, we do not know whether increased inhibitory receptor expression could influence T<sub>RM</sub> functionality at lower peptide concentrations. Our results also demonstrate that primary and repetitively stimulated brain T<sub>RM</sub> can protect against an antigen-congruent bacterial challenge. Future explorations could exhibit disparate outcomes on the basis of the pathogen selected for rechallenge, as has previously been observed for repetitively stimulated T<sub>CIRCM</sub>.<sup>23</sup> Finally, the potentially pathogenic consequences of resting or reactivated brain T<sub>RM</sub> seeded by multiple peripheral infections is unclear. Thus, future studies of repetitively stimulated brain T<sub>RM</sub> will require consideration of host, pathogen, time, and tissue-intrinsic variables.

### RESOURCE AVAILABILITY

#### Lead contact

Further information and requests for resources and reagents should be directed to and will be fulfilled by the lead contact, John T. Harty ([john-harty@uiowa.edu](mailto:john-harty@uiowa.edu)).

Experiments in (A)–(D) show data from 3 of 3 independent experiments with  $n = 15\text{--}20$  mice per group. Experiments in (E)–(H) show data from 2 of 2 experiments with  $n = 8\text{--}9$  mice per group. Experiments in (I) show one representative image from  $n = 2$  replicate mice. Experiments in (J)–(M) show data from 2 of 2 experiments with  $n = 6\text{--}7$  mice per group. Statistical significance was determined by paired t test, Student's t test, or one-way ANOVA with Tukey's multiple comparisons post-test using GraphPad Prism. Graphs show the mean  $\pm$  SEM, with each symbol representing one mouse. Individual  $p$  values are noted on the respective graphs. Scale bar: 200  $\mu\text{m}$ . Graphical illustrations were created using BioRender (<https://biorender.com>).

### Materials availability

Many reagents and mice used in this study are available for purchase from the listed vendors. Reagents and organisms unique to this study may be available, with shipping fees paid by the requesting lab, upon request to the lead contact. Available materials include bacteria and viruses.

### Data and code availability

- All data reported in this paper will be shared by the lead contact upon request.
- This paper does not report original code.
- Any additional information required to reanalyze the data reported in this paper is available from the lead contact upon request.

### ACKNOWLEDGMENTS

We thank members of the Harty and Badovinac laboratories for valuable discussions. We thank Ivan Badovinac, Jack Harty (no relation to J.T.H.), and Zachary Darr for maintaining laboratory solutions and equipment. We are thankful to the laboratory of Alexander Bassuk for sharing their slide-scanning microscope for image procurement. The graphical illustrations in the figures were created using BioRender (<https://biorender.com>). This work was funded by National Institutes of Health grants R01AI042767 (J.T.H.), R01AI167847 (J.T.H.), R21AI178159 (J.T.H.), R21AI185067 (J.T.H.), R01AI114543 (J.T.H. and V.P.B.), R35GM134880 (V.P.B.), T32AI007260 (C.E.F.), and T32GM139776 (M.R.M. and S.A.A.) and the University of Iowa Graduate College Post-Comprehensive Research Fellowship (M.R.M.).

### AUTHOR CONTRIBUTIONS

Conceptualization, M.R.M., V.P.B., and J.T.H.; methodology, M.R.M., S.v.d.W., M.H., E.A.E., C.E.F., L.L.P., L.S.H., V.P.B., and J.T.H.; investigation, M.R.M., S.v.d.W., M.H., E.A.E., C.E.F., L.L.P., L.S.H., S.A.A., and C.M.S.; visualization, M.R.M. and J.T.H.; funding acquisition, V.P.B. and J.T.H.; project administration, V.P.B. and J.T.H.; supervision, V.P.B. and J.T.H.; writing – original draft, M.R.M., V.P.B., and J.T.H.; writing – review & editing, M.R.M., S.v.d.W., M.H., E.A.E., C.E.F., L.L.P., L.S.H., S.A.A., C.M.S., V.P.B., and J.T.H.

### DECLARATION OF INTERESTS

The authors declare no competing interests.

### STAR METHODS

Detailed methods are provided in the online version of this paper and include the following:

- KEY RESOURCES TABLE
- EXPERIMENTAL MODEL AND STUDY PARTICIPANT DETAILS
  - Mice
  - Adoptive transfer
  - Infections
  - Antibody depletion and FTY720 treatment
- METHOD DETAILS
  - Tissue collection and cellular isolation
  - Cell staining and flow cytometry
  - Immunohistochemistry
  - Bacterial counts
- QUANTIFICATION AND STATISTICAL ANALYSIS

## SUPPLEMENTAL INFORMATION

Supplemental information can be found online at <https://doi.org/10.1016/j.celrep.2025.115247>.

Received: July 29, 2024

Revised: December 17, 2024

Accepted: January 9, 2025

Published: February 3, 2025

## REFERENCES

1. Kipnis, J., and Filiano, A.J. (2018). Neuroimmunology in 2017: The central nervous system: privileged by immune connections. *Nat. Rev. Immunol.* 18, 83–84. <https://doi.org/10.1038/nri.2017.152>.
2. Yoshida, T.M., Wang, A., and Hafler, D.A. (2022). Basic principles of neuroimmunology. *Semin. Immunopathol.* 44, 685–695. <https://doi.org/10.1007/s00281-022-00951-7>.
3. Paolicelli, R.C., Sierra, A., Stevens, B., Tremblay, M.E., Aguzzi, A., Ajami, B., Amit, I., Audinat, E., Bechmann, I., Bennett, M., et al. (2022). Microglia states and nomenclature: A field at its crossroads. *Neuron* 110, 3458–3483. <https://doi.org/10.1016/j.neuron.2022.10.020>.
4. Castellani, G., Croese, T., Peralta Ramos, J.M., and Schwartz, M. (2023). Transforming the understanding of brain immunity. *Science* 380, eabo7649. <https://doi.org/10.1126/science.abo7649>.
5. Ai, S., and Klein, R.S. (2020). Update on T cells in the virally infected brain: friends and foes. *Curr. Opin. Neurol.* 33, 405–412. <https://doi.org/10.1097/WCO.0000000000000825>.
6. Mix, M.R., and Harty, J.T. (2022). Keeping T cell memories in mind. *Trends Immunol.* 43, 1018–1031. <https://doi.org/10.1016/j.it.2022.10.001>.
7. Wakim, L.M., Woodward-Davis, A., and Bevan, M.J. (2010). Memory T cells persisting within the brain after local infection show functional adaptations to their tissue of residence. *Proc. Natl. Acad. Sci. USA* 107, 17872–17879. <https://doi.org/10.1073/pnas.1012021107>.
8. Wakim, L.M., Woodward-Davis, A., Liu, R., Hu, Y., Villadangos, J., Smyth, G., and Bevan, M.J. (2012). The molecular signature of tissue resident memory CD8 T cells isolated from the brain. *J. Immunol.* 189, 3462–3471. <https://doi.org/10.4049/jimmunol.1201305>.
9. Monje, M., and Iwasaki, A. (2022). The neurobiology of long COVID. *Neuron* 110, 3484–3496. <https://doi.org/10.1016/j.neuron.2022.10.006>.
10. Ayasoufi, K., Wolf, D., Namen, S., Tritz, Z., Jin, F., Pfaller, C., Goddery, E., Fain, C., Gulbicki, L., Khadka, R., et al. (2022). Brain resident memory T cells rapidly expand and initiate neuroinflammatory responses following CNS injury and viral infection. *bioRxiv* 2022, 487707. <https://doi.org/10.1101/2022.04.08.487707>.
11. Ning, J., Gavil, N.V., Wu, S., Wijeyesinghe, S., Weyu, E., Ma, J., Li, M., Grigore, F.N., Dhawan, S., Skorput, A.G.J., et al. (2022). Functional virus-specific memory T cells survey glioblastoma. *Cancer Immunol. Immunother.* 71, 1863–1875. <https://doi.org/10.1007/s00262-021-03125-w>.
12. Steinbach, K., Vincenti, I., Egervari, K., Kreutzfeldt, M., van der Meer, F., Page, N., Klimek, B., Rossitto-Borlat, I., Di Liberto, G., Muschawecckh, A., et al. (2019). Brain-resident memory T cells generated early in life predispose to autoimmune disease in mice. *Sci. Transl. Med.* 11, eaav5519. <https://doi.org/10.1126/scitranslmed.aav5519>.
13. Urban, S.L., Jensen, I.J., Shan, Q., Pewe, L.L., Xue, H.H., Badovinac, V.P., and Harty, J.T. (2020). Peripherally induced brain tissue-resident memory CD8(+) T cells mediate protection against CNS infection. *Nat. Immunol.* 21, 938–949. <https://doi.org/10.1038/s41590-020-0711-8>.
14. Steinbach, K., Vincenti, I., Kreutzfeldt, M., Page, N., Muschawecckh, A., Wagner, I., Drexler, I., Pinschewer, D., Korn, T., and Merkler, D. (2016). Brain-resident memory T cells represent an autonomous cytotoxic barrier to viral infection. *J. Exp. Med.* 213, 1571–1587. <https://doi.org/10.1084/jem.20151916>.
15. Garber, C., Soung, A., Vollmer, L.L., Kanmogne, M., Last, A., Brown, J., and Klein, R.S. (2019). T cells promote microglia-mediated synaptic elimination and cognitive dysfunction during recovery from neuropathogenic flaviviruses. *Nat. Neurosci.* 22, 1276–1288. <https://doi.org/10.1038/s41593-019-0427-y>.
16. Rosen, S.F., Soung, A.L., Yang, W., Ai, S., Kanmogne, M., Davé, V.A., Artyomov, M., Magee, J.A., and Klein, R.S. (2022). Single-cell RNA transcriptome analysis of CNS immune cells reveals CXCL16/CXCR6 as maintenance factors for tissue-resident T cells that drive synapse elimination. *Genome Med.* 14, 108. <https://doi.org/10.1186/s13073-022-01111-0>.
17. Landrith, T.A., Sureshchandra, S., Rivera, A., Jang, J.C., Rais, M., Nair, M.G., Messaoudi, I., and Wilson, E.H. (2017). CD103(+) CD8 T Cells in the Toxoplasma-Infected Brain Exhibit a Tissue-Resident Memory Transcriptional Profile. *Front. Immunol.* 8, 335. <https://doi.org/10.3389/fimmu.2017.00335>.
18. Shallberg, L.A., Phan, A.T., Christian, D.A., Perry, J.A., Haskins, B.E., Beiting, D.P., Harris, T.H., Koshy, A.A., and Hunter, C.A. (2022). Impact of secondary TCR engagement on the heterogeneity of pathogen-specific CD8+ T cell response during acute and chronic toxoplasmosis. *PLoS Pathog.* 18, e1010296. <https://doi.org/10.1371/journal.ppat.1010296>.
19. Musial, S.C., Kleist, S.A., Degefu, H.N., Ford, M.A., Chen, T., Isaacs, J.F., Boussiotti, V.A., Skorput, A.G.J., and Rosato, P.C. (2024). Alarm functions of PD-1+ brain resident memory T cells. *bioRxiv* 2024, 1585–1594. <https://doi.org/10.1101/2024.06.06.597370>.
20. Fernandez-Castaneda, A., Lu, P., Geraghty, A.C., Song, E., Lee, M.H., Wood, J., O'Dea, M.R., Dutton, S., Shamardani, K., Nwangwu, K., et al. (2022). Mild respiratory COVID can cause multi-lineage neural cell and myelin dysregulation. *Cell* 185, 2452–2468. <https://doi.org/10.1016/j.cell.2022.06.008>.
21. Wirth, T.C., Xue, H.H., Rai, D., Sabel, J.T., Bair, T., Harty, J.T., and Badovinac, V.P. (2010). Repetitive antigen stimulation induces stepwise transcriptome diversification but preserves a core signature of memory CD8(+) T cell differentiation. *Immunity* 33, 128–140. <https://doi.org/10.1016/j.immuni.2010.06.014>.
22. Wirth, T.C., Martin, M.D., Starbeck-Miller, G., Harty, J.T., and Badovinac, V.P. (2011). Secondary CD8+ T-cell responses are controlled by systemic inflammation. *Eur. J. Immunol.* 41, 1321–1333. <https://doi.org/10.1002/eji.201040730>.
23. Nolz, J.C., and Harty, J.T. (2011). Protective capacity of memory CD8+ T cells is dictated by antigen exposure history and nature of the infection. *Immunity* 34, 781–793. <https://doi.org/10.1016/j.immuni.2011.03.020>.
24. Martin, M.D., and Badovinac, V.P. (2014). Influence of time and number of antigen encounters on memory CD8 T cell development. *Immunol. Res.* 59, 35–44. <https://doi.org/10.1007/s12026-014-8522-3>.
25. Rai, D., Martin, M.D., and Badovinac, V.P. (2014). The longevity of memory CD8 T cell responses after repetitive antigen stimulations. *J. Immunol.* 192, 5652–5659. <https://doi.org/10.4049/jimmunol.1301063>.
26. Martin, M.D., and Badovinac, V.P. (2015). Antigen-dependent and -independent contributions to primary memory CD8 T cell activation and protection following infection. *Sci. Rep.* 5, 18022. <https://doi.org/10.1038/srep18022>.
27. Van Braeckel-Budimir, N., Martin, M.D., Hartwig, S.M., Legge, K.L., Badovinac, V.P., and Harty, J.T. (2017). Antigen Exposure History Defines CD8 T Cell Dynamics and Protection during Localized Pulmonary Infections. *Front. Immunol.* 8, 40. <https://doi.org/10.3389/fimmu.2017.00040>.
28. Van Braeckel-Budimir, N., Varga, S.M., Badovinac, V.P., and Harty, J.T. (2018). Repeated Antigen Exposure Extends the Durability of Influenza-Specific Lung-Resident Memory CD8(+) T Cells and Heterosubtypic Immunity. *Cell Rep.* 24, 3374–3382. <https://doi.org/10.1016/j.celrep.2018.08.073>.
29. Anthony, S.M., Van Braeckel-Budimir, N., Moioffer, S.J., van de Wall, S., Shan, Q., Vijay, R., Sompallae, R., Hartwig, S.M., Jensen, I.J., Varga, S.M., et al. (2021). Protective function and durability of mouse lymph

- node-resident memory CD8(+) T cells. *Elife* 10, e68662. <https://doi.org/10.7554/eLife.68662>.
30. Nelson, C.E., Thompson, E.A., Quarnstrom, C.F., Fraser, K.A., Seelig, D.M., Bhela, S., Burbach, B.J., Masopust, D., and Vezys, V. (2019). Robust Iterative Stimulation with Self-Antigens Overcomes CD8(+) T Cell Tolerance to Self- and Tumor Antigens. *Cell Rep.* 28, 3092–3104. <https://doi.org/10.1016/j.celrep.2019.08.038>.
  31. Danahy, D.B., Berton, R.R., and Badovinac, V.P. (2020). Cutting Edge: Antitumor Immunity by Pathogen-Specific CD8 T Cells in the Absence of Cognate Antigen Recognition. *J. Immunol.* 204, 1431–1435. <https://doi.org/10.4049/jimmunol.1901172>.
  32. Soerens, A.G., Kunzli, M., Quarnstrom, C.F., Scott, M.C., Swanson, L., Locquiao, J.J., Ghoneim, H.E., Zehn, D., Youngblood, B., Vezys, V., and Masopust, D. (2023). Functional T cells are capable of supernumerary cell division and longevity. *Nature* 614, 762–766. <https://doi.org/10.1038/s41586-022-05626-9>.
  33. Masopust, D., and Soerens, A.G. (2019). Tissue-Resident T Cells and Other Resident Leukocytes. *Annu. Rev. Immunol.* 37, 521–546. <https://doi.org/10.1146/annurev-immunol-042617-053214>.
  34. Yeniyuwadee, S., Sanchez-Trincado Lopez, J.L., Shah, R., Rosato, P.C., and Boussiatis, V.A. (2022). The evolving role of tissue-resident memory T cells in infections and cancer. *Sci. Adv.* 8, eab05871. <https://doi.org/10.1126/sciadv.ab05871>.
  35. Lam, N., Lee, Y., and Farber, D.L. (2024). A guide to adaptive immune memory. *Nat. Rev. Immunol.* 24, 810–829. <https://doi.org/10.1038/s41577-024-01040-6>.
  36. Gray, J.I., and Farber, D.L. (2022). Tissue-Resident Immune Cells in Humans. *Annu. Rev. Immunol.* 40, 195–220. <https://doi.org/10.1146/annurev-immunol-093019-112809>.
  37. Martin, M.D., and Badovinac, V.P. (2018). Defining Memory CD8 T Cell. *Front. Immunol.* 9, 2692. <https://doi.org/10.3389/fimmu.2018.02692>.
  38. Ning, J., Gavil, N.V., Wu, S., Wijeyesinghe, S., Weyu, E., Ma, J., Li, M., Grigore, F.N., Dhawan, S., Skorput, A.G.J., et al. (2022). Functional virus-specific memory T cells survey glioblastoma. *Cancer Immunol. Immunother.* 71, 1863–1875. <https://doi.org/10.1007/s00262-021-03125-w>.
  39. Casey, K.A., Fraser, K.A., Schenkel, J.M., Moran, A., Abt, M.C., Beura, L.K., Lucas, P.J., Artis, D., Wherry, E.J., Hogquist, K., et al. (2012). Antigen-independent differentiation and maintenance of effector-like resident memory T cells in tissues. *J. Immunol.* 188, 4866–4875. <https://doi.org/10.4049/jimmunol.1200402>.
  40. Frieser, D., Pignata, A., Khajavi, L., Shlesinger, D., Gonzalez-Fierro, C., Nguyen, X.H., Yermanos, A., Merkler, D., Höftberger, R., Desestret, V., et al. (2022). Tissue-resident CD8(+) T cells drive compartmentalized and chronic autoimmune damage against CNS neurons. *Sci. Transl. Med.* 14, eabl6157. <https://doi.org/10.1126/scitranslmed.abl6157>.
  41. Gate, D., Saligrama, N., Leventhal, O., Yang, A.C., Unger, M.S., Middendorp, J., Chen, K., Lehallier, B., Channappa, D., De Los Santos, M.B., et al. (2020). Clonally expanded CD8 T cells patrol the cerebrospinal fluid in Alzheimer's disease. *Nature* 577, 399–404. <https://doi.org/10.1038/s41586-019-1895-7>.
  42. Chang, J.W., Reyes, S.D., Faure-Kumar, E., Lam, S.K., Lawlor, M.W., Leventer, R.J., Lew, S.M., Lockhart, P.J., Pope, K., Weiner, H.L., et al. (2021). Clonally Focused Public and Private T Cells in Resected Brain Tissue From Surgeries to Treat Children With Intractable Seizures. *Front. Immunol.* 12, 664344. <https://doi.org/10.3389/fimmu.2021.664344>.
  43. Schenkel, J.M., Fraser, K.A., Vezys, V., and Masopust, D. (2013). Sensing and alarm function of resident memory CD8(+) T cells. *Nat. Immunol.* 14, 509–513. <https://doi.org/10.1038/ni.2568>.
  44. Boni, M.F. (2008). Vaccination and antigenic drift in influenza. *Vaccine* 26, C8–C14. <https://doi.org/10.1016/j.vaccine.2008.04.011>.
  45. Anderson, K.G., Mayer-Barber, K., Sung, H., Beura, L., James, B.R., Taylor, J.J., Qunaj, L., Griffith, T.S., Vezys, V., Barber, D.L., and Masopust, D. (2014). Intravascular staining for discrimination of vascular and tissue leukocytes. *Nat. Protoc.* 9, 209–222. <https://doi.org/10.1038/nprot.2014.005>.
  46. Wherry, E.J., Blattman, J.N., Murali-Krishna, K., van der Most, R., and Ahmed, R. (2003). Viral persistence alters CD8 T-cell immunodominance and tissue distribution and results in distinct stages of functional impairment. *J. Virol.* 77, 4911–4927. <https://doi.org/10.1128/jvi.77.8.4911-4927.2003>.
  47. Kenney, L.L., Carter, E.P., Gil, A., and Selin, L.K. (2021). T cells in the brain enhance neonatal mortality during peripheral LCMV infection. *PLoS Pathog.* 17, e1009066. <https://doi.org/10.1371/journal.ppat.1009066>.
  48. Pappalardo, J.L., Zhang, L., Pecsok, M.K., Perlman, K., Zografou, C., Rad dassi, K., Abulaban, A., Krishnaswamy, S., Antel, J., van Dijk, D., and Hafler, D.A. (2020). Transcriptomic and clonal characterization of T cells in the human central nervous system. *Sci. Immunol.* 5, eabb8786. <https://doi.org/10.1126/sciimmunol.abb8786>.
  49. Smolders, J., Heutink, K.M., Fransen, N.L., Remmerswaal, E.B.M., Hombrink, P., Ten Berge, I.J.M., van Lier, R.A.W., Huitinga, I., and Hamann, J. (2018). Tissue-resident memory T cells populate the human brain. *Nat. Commun.* 9, 4593. <https://doi.org/10.1038/s41467-018-07053-9>.
  50. McLane, L.M., Abdel-Hakeem, M.S., and Wherry, E.J. (2019). CD8 T Cell Exhaustion During Chronic Viral Infection and Cancer. *Annu. Rev. Immunol.* 37, 457–495. <https://doi.org/10.1146/annurev-immunol-041015-055318>.
  51. Hayward, S.L., Scharer, C.D., Cartwright, E.K., Takamura, S., Li, Z.R.T., Boss, J.M., and Kohlmeier, J.E. (2020). Environmental cues regulate epigenetic reprogramming of airway-resident memory CD8(+) T cells. *Nat. Immunol.* 21, 309–320. <https://doi.org/10.1038/s41590-019-0584-x>.
  52. Cheuk, S., Schlums, H., Gallais Séréal, I., Martini, E., Chiang, S.C., Marquardt, N., Gibbs, A., Detloffson, E., Introini, A., Forkel, M., et al. (2017). CD49a Expression Defines Tissue-Resident CD8(+) T Cells Poised for Cytotoxic Function in Human Skin. *Immunity* 46, 287–300. <https://doi.org/10.1016/j.immuni.2017.01.009>.
  53. Watanabe, R., Gehad, A., Yang, C., Scott, L.L., Teague, J.E., Schlapbach, C., Elco, C.P., Huang, V., Matos, T.R., Kupper, T.S., and Clark, R.A. (2015). Human skin is protected by four functionally and phenotypically discrete populations of resident and recirculating memory T cells. *Sci. Transl. Med.* 7, 279ra39. <https://doi.org/10.1126/scitranslmed.3010302>.
  54. Dijkgraaf, F.E., Matos, T.R., Hoogenboezem, M., Toebees, M., Vredevoogd, D.W., Mertz, M., van den Broek, B., Song, J.Y., Teunissen, M.B.M., Luiten, R.M., et al. (2019). Tissue patrol by resident memory CD8(+) T cells in human skin. *Nat. Immunol.* 20, 756–764. <https://doi.org/10.1038/s41590-019-0404-3>.
  55. Bartolome-Casado, R., Landsverk, O.J.B., Chauhan, S.K., Richter, L., Phung, D., Greiff, V., Risnes, L.F., Yao, Y., Neumann, R.S., Yaqub, S., et al. (2019). Resident memory CD8 T cells persist for years in human small intestine. *J. Exp. Med.* 216, 2412–2426. <https://doi.org/10.1084/jem.20190414>.
  56. Christo, S.N., Evrard, M., Park, S.L., Gandolfo, L.C., Burn, T.N., Fonseca, R., Newman, D.M., Alexandre, Y.O., Collins, N., Zamudio, N.M., et al. (2021). Discrete tissue microenvironments instruct diversity in resident memory T cell function and plasticity. *Nat. Immunol.* 22, 1140–1151. <https://doi.org/10.1038/s41590-021-01004-1>.
  57. Fonseca, R., Burn, T.N., Gandolfo, L.C., Devi, S., Park, S.L., Obers, A., Evrard, M., Christo, S.N., Buquicchio, F.A., Lareau, C.A., et al. (2022). Runx3 drives a CD8(+) T cell tissue residency program that is absent in CD4(+) T cells. *Nat. Immunol.* 23, 1236–1245. <https://doi.org/10.1038/s41590-022-01273-4>.
  58. Slutter, B., Van Braeckel-Budimir, N., Abboud, G., Varga, S.M., Salek-Ardakani, S., and Harty, J.T. (2017). Dynamics of influenza-induced lung-resident memory T cells underlie waning heterosubtypic immunity. *Sci. Immunol* 2, eaag2031. <https://doi.org/10.1126/sciimmunol.aag2031>.
  59. Dulken, B.W., Buckley, M.T., Navarro Negredo, P., Saligrama, N., Cayrol, R., Leeman, D.S., George, B.M., Boutet, S.C., Hebestreit, K., Pluvinage, J.V., et al. (2019). Single-cell analysis reveals T cell infiltration in old

- neurogenic niches. *Nature* 571, 205–210. <https://doi.org/10.1038/s41586-019-1362-5>.
60. Fain, C.E., Zheng, J., Jin, F., Ayasoufi, K., Wu, Y., Lilley, M.T., Dropik, A.R., Wolf, D.M., Rodriguez, R.C., Albaidula, A., et al. (2024). Discrete class I molecules on brain endothelium differentially regulate neuropathology in experimental cerebral malaria. *Brain* 147, 566–589. <https://doi.org/10.1093/brain/awad319>.
  61. Swanson, P.A., 2nd, Hart, G.T., Russo, M.V., Nayak, D., Yazew, T., Peña, M., Khan, S.M., Janse, C.J., Pierce, S.K., and McGavern, D.B. (2016). CD8+ T Cells Induce Fatal Brainstem Pathology during Cerebral Malaria via Luminal Antigen-Specific Engagement of Brain Vasculature. *PLoS Pathog.* 12, e1006022. <https://doi.org/10.1371/journal.ppat.1006022>.
  62. Prat, A., Biernacki, K., Becher, B., and Antel, J.P. (2000). B7 expression and antigen presentation by human brain endothelial cells: requirement for proinflammatory cytokines. *J. Neuropathol. Exp. Neurol.* 59, 129–136. <https://doi.org/10.1093/jnen/59.2.129>.
  63. Etienne, S., Bourdoulous, S., Strosberg, A.D., and Couraud, P.O. (1999). MHC class II engagement in brain endothelial cells induces protein kinase A-dependent IL-6 secretion and phosphorylation of cAMP response element-binding protein. *J. Immunol.* 163, 3636–3641.
  64. Lucas, E.D., Huggins, M.A., Peng, C., O'Connor, C., Gress, A.R., Thefaine, C.E., Dehm, E.M., Kubota, Y., Jameson, S.C., and Hamilton, S.E. (2024). Circulating KLRG1(+) long-lived effector memory T cells retain the flexibility to become tissue resident. *Sci. Immunol.* 9, eadj8356. <https://doi.org/10.1126/sciimmunol.adj8356>.
  65. Goldberg, L., Haas, E.R., Urak, R., Vyas, V., Pathak, K.V., Garcia-Mansfield, K., Pirrotte, P., Singhal, J., Figarola, J.L., Aldoss, I., et al. (2024). Immunometabolic Adaptation of CD19-Targeted CAR T Cells in the Central Nervous System Microenvironment of Patients Promotes Memory Development. *Cancer Res.* 84, 1048–1064. <https://doi.org/10.1158/0008-5472.CAN-23-2299>.
  66. Portnow, J., Wang, D., Blanchard, M.S., Tran, V., Alizadeh, D., Starr, R., Dodia, R., Chiu, V., Brito, A., Kilpatrick, J., et al. (2020). Systemic Anti-PD-1 Immunotherapy Results in PD-1 Blockade on T Cells in the Cerebrospinal Fluid. *JAMA Oncol.* 6, 1947–1951. <https://doi.org/10.1001/jamaoncol.2020.4508>.
  67. Bernard-Valnet, R., Frieser, D., Nguyen, X.H., Khajavi, L., Quériault, C., Arthaud, S., Melzi, S., Fusade-Boyer, M., Masson, F., Zytnicki, M., et al. (2022). Influenza vaccination induces autoimmunity against orexinergic neurons in a mouse model for narcolepsy. *Brain* 145, 2018–2030. <https://doi.org/10.1093/brain/awab455>.
  68. Bernard-Valnet, R., Yshii, L., Quériault, C., Nguyen, X.H., Arthaud, S., Rodrigues, M., Canivet, A., Morel, A.L., Matthys, A., Bauer, J., et al. (2016). CD8 T cell-mediated killing of orexinergic neurons induces a narcolepsy-like phenotype in mice. *Proc. Natl. Acad. Sci. USA* 113, 10956–10961. <https://doi.org/10.1073/pnas.1603251113>.
  69. van Nierop, G.P., van Luijn, M.M., Michels, S.S., Melief, M.J., Janssen, M., Langerak, A.W., Ouwendijk, W.J.D., Hintzen, R.Q., and Verjans, G.M.G.M. (2017). Phenotypic and functional characterization of T cells in white matter lesions of multiple sclerosis patients. *Acta Neuropathol.* 134, 383–401. <https://doi.org/10.1007/s00401-017-1744-4>.
  70. Bjornevik, K., Cortese, M., Healy, B.C., Kuhle, J., Mina, M.J., Leng, Y., Elledge, S.J., Niebuhr, D.W., Scher, A.I., Munger, K.L., and Ascherio, A. (2022). Longitudinal analysis reveals high prevalence of Epstein-Barr virus associated with multiple sclerosis. *Science* 375, 296–301. <https://doi.org/10.1126/science.abj8222>.
  71. Chen, X., Firulyova, M., Manis, M., Herz, J., Smirnov, I., Aladyeva, E., Wang, C., Bao, X., Finn, M.B., Hu, H., et al. (2023). Microglia-mediated T cell infiltration drives neurodegeneration in tauopathy. *Nature* 615, 668–677. <https://doi.org/10.1038/s41586-023-05788-0>.
  72. Cassidy, B.R., Logan, S., Farley, J.A., Owen, D.B., Sonntag, W.E., and Drevets, D.A. (2023). Progressive cognitive impairment after recovery from neuroinvasive and non-neuroinvasive *Listeria monocytogenes* infection. *Front. Immunol.* 14, 1146690. <https://doi.org/10.3389/fimmu.2023.1146690>.
  73. Cassidy, B.R., Sonntag, W.E., Leenen, P.J.M., and Drevets, D.A. (2022). Systemic *Listeria monocytogenes* infection in aged mice induces long-term neuroinflammation: the role of miR-155. *Immun. Ageing* 19, 25. <https://doi.org/10.1186/s12979-022-00281-0>.
  74. Altendorfer, B., Unger, M.S., Poupadrin, R., Hoog, A., Asslaber, D., Gratz, I.K., Mrowetz, H., Benedetti, A., de Sousa, D.M.B., Greil, R., et al. (2022). Transcriptomic Profiling Identifies CD8(+) T Cells in the Brain of Aged and Alzheimer's Disease Transgenic Mice as Tissue-Resident Memory T Cells. *J. Immunol.* 209, 1272–1285. <https://doi.org/10.4049/jimmunol.2100737>.
  75. Jorfi, M., Park, J., Hall, C.K., Lin, C.C.J., Chen, M., von Maydell, D., Kruskop, J.M., Kang, B., Choi, Y., Prokopenko, D., et al. (2023). Infiltrating CD8(+) T cells exacerbate Alzheimer's disease pathology in a 3D human neuroimmune axis model. *Nat. Neurosci.* 26, 1489–1504. <https://doi.org/10.1038/s41593-023-01415-3>.
  76. Sun, E.D., Zhou, O.Y., Hauptschein, M., Rapoport, N., Xu, L., Navarro Negredo, P., Liu, L., Rando, T.A., Zou, J., and Brunet, A. (2024). Spatial transcriptomic clocks reveal cell proximity effects in brain ageing. *Nature* 1–12. <https://doi.org/10.1038/s41586-024-08334-8>.
  77. Mueller, S.N., Langley, W.A., Li, G., García-Sastre, A., Webb, R.J., and Ahmed, R. (2010). Qualitatively different memory CD8+ T cells are generated after lymphocytic choriomeningitis virus and influenza virus infections. *J. Immunol.* 185, 2182–2190. <https://doi.org/10.4049/jimmunol.1001142>.

## STAR★METHODS

### KEY RESOURCES TABLE

REAGENT or RESOURCE	SOURCE	IDENTIFIER
<b>Antibodies</b>		
BV785 anti-mouse CD8a (53–6.7)	BioLegend	Cat #100750; RRID: AB_2562610
PE anti-mouse CD8a (53–6.7)	BioLegend	Cat #100708; RRID: AB_312747
Alexa Fluor 700 anti-mouse CD90.1 (OX-7)	BioLegend	Cat #202528; RRID: AB_1626241
APC anti-mouse CD90.1 (OX-7)	BioLegend	Cat #202526; RRID: AB_1595470
FITC anti-mouse CD90.1 (OX-7)	BioLegend	Cat #202504; RRID: AB_1595653
PE anti-mouse CD90.1 (OX-7)	BioLegend	Cat #202524; RRID: AB_1595524
Alexa Fluor 700 anti-mouse CD90.2 (53–2.1)	BioLegend	Cat #105320; RRID: AB_493725
FITC anti-mouse CD90.2 (53–2.1)	BioLegend	Cat #140304; RRID: AB_10642812
PE/Cy7 anti-mouse CD90.2 (53–2.1)	eBio	Cat #25-0902-82; RRID: AB_469642
FITC anti-mouse CD11a (2D7)	BioLegend	Cat #101106; RRID: AB_312779
BV510 anti-mouse CD11a (2D7)	BD Biosciences	Cat #740110; RRID: AB_2739868
PE/CF594 anti-mouse CD69 (H1.2F3)	BD Biosciences	Cat #562455; RRID: AB_11154217
BB700 anti-mouse CD49a (Ha31/8)	BD Biosciences	Cat #742164; RRID: AB_2861198
PE anti-mouse CXCR6 (SA051D1)	BioLegend	Cat #151104; RRID: AB_2566546
BV421 anti-mouse CXCR3 (CXCR3-173)	BioLegend	Cat #126522; RRID: AB_2562205
BV421 anti-mouse PD-1 (29F.1A12)	BioLegend	Cat #135221; RRID: AB_2562568
PE anti-mouse TOX (REA473)	Miltenyi	Cat #130-120-785; RRID: AB_2801780
PerCP/eF710 anti-mouse LAG-3 (C9B7W)	eBio	Cat #46-2231-82; RRID: AB_11151334
APC anti-mouse CD45 (30-F11)	BioLegend	Cat #103112; RRID: AB_312977
Pacific Blue anti-mouse CD45 (30-F11)	BioLegend	Cat #103126; RRID: AB_493535
BV421 anti-mouse CD45.2 (104)	BioLegend	Cat #109832; RRID: AB_2565511
PE/Cy7 anti-mouse CD11b (M1/70)	BioLegend	Cat #101216; RRID: AB_312799
BV510 anti-mouse B220 (RA3-6B2)	BioLegend	Cat #103248; RRID: AB_2650679
PerCp/Cy5.5 anti-mouse CD138 (281-2)	BioLegend	Cat #142510; RRID: AB_2561601
PE anti-mouse CD138 (281-2)	BioLegend	Cat #142504; RRID: AB_10916119
PE anti-mouse CD4 (H129.19)	BioLegend	Cat #130310; RRID: AB_2075573
FITC anti-mouse CD4 (H129.19)	BioLegend	Cat #130308; RRID: AB_1279237
PerCP anti-mouse CD4 (L3T4/RM4-5)	BD Biosciences	Cat #553052; RRID: AB_394587
PE/CF594 anti-mouse CD11c (N418)	BioLegend	Cat #117347; RRID: 117348
FITC anti-mouse NKp46 (29A1.4)	BioLegend	Cat #137606; RRID: AB_2298210
PE anti-mouse NKp46 (29A1.4)	BioLegend	Cat #137604; RRID: AB_2235755
PerCpE/F710 anti-mouse NKp46 (29A1.4)	eBio	Cat #46-3351-82; RRID: AB_1834441
APC anti-mouse Ly6C (HK1.4)	BioLegend	Cat #128016; RRID: AB_1732076
APC anti-mouse TCR $\beta$ (H57-597)	BioLegend	Cat #109212; RRID: AB_313434
Alexa Fluor 700 anti-mouse Ly6G (1A8)	BioLegend	Cat #127622; RRID: AB_10643269
BV421 anti-mouse IFN- $\gamma$ (XMG1.2)	BioLegend	Cat #505830; RRID: AB_2563105
PE/Cy7 anti-mouse TNF (MP6-XT22)	BioLegend	Cat #506324; RRID: AB_2256076
FITC anti-mouse Granzyme B (GB11)	BioLegend	Cat #515403; RRID: AB_2114575
PE anti-mouse CD107a (1D4B)	BioLegend	Cat #121612; RRID: AB_1732051
APC/eF780 fixable viability stain	BD Biosciences	Cat #565388; RRID: AB_2869673
a-Thy1.1 (19E12)	BioXcell	Cat #BE0214; RRID: AB_2687700
24.2G Fc Block	Harty lab	NA

(Continued on next page)

**Continued**

REAGENT or RESOURCE	SOURCE	IDENTIFIER
<b>Bacterial and virus strains</b>		
Recombinant influenza PR8-GP33 virus	Harty lab	NA
Lymphocytic choriomeningitis virus (LCMV) strain Armstrong	Harty lab	NA
<i>Listeria monocytogenes</i> expressing -GP33, attenuated ( $\Delta$ actA, $\Delta$ InlB-deficient)	Harty lab	NA
<i>Listeria monocytogenes</i> expressing -GAP50, attenuated ( $\Delta$ actA, $\Delta$ InlB-deficient)	Harty lab	NA
<b>Chemicals, peptides, and recombinant proteins</b>		
ACK lysis buffer	Harty lab	NA
Vitalyse	CMDG	Cat #WBL0100
Collagenase D	Millipore Sigma	Cat #11088866001
Collagenase II	Millipore Sigma	Cat #17101015
DNase	Millipore Sigma	Cat #D4513-1VL
Percoll	GE Healthcare	Cat #17-0891-01
HEPES	Gibco	Cat #15630080
DPBS	Gibco	Cat #14190144
RPMI	Gibco	Cat #11875093
DMEM	Gibco	Cat #11965092
HBSS	Gibco	Cat #14025092
FACS Buffer	Harty lab	NA
Cytofix Fixation Buffer	BD Bioscience	Cat #554655
Igepal	Millipore Sigma	Cat #56741
Tryptic Soy Broth	BD Bioscience	Cat #BA-257107.06
Low Melting Point Agarose	Promega	Cat #V2111
GP <sub>33-41</sub> peptide	Global Peptide	KAVYNFATC
FTY720	Millipore Sigma	Cat #SML0700
ProLong <sup>TM</sup> Gold Antifade Mountant with DAPI	Thermo Fisher	Cat #P36935
<b>Critical commercial assays</b>		
CountBright <sup>TM</sup> Absolute Counting Beads, for flow cytometry	Thermo Fisher	Cat #C36950
FoxP3/Transcription Factor Staining Kit	Tonbo/Cytek	Cat #SKU TNB-0607-KIT
Anti-PE MicroBeads	Miltenyi Biotec	Cat #130-048-801
Tumor Dissociation Kit, mouse	Miltenyi Biotec	Cat #130-096-730
Debris Removal Solution	Miltenyi Biotec	Cat #130-109-398
<b>Experimental models: Organisms/strains</b>		
C57BL/6NCrl	Charles River	Strain Code 027
P14	Jackson Laboratories	037394
Thy1.1	Jackson Laboratories	000406
P14 Thy1.1/1 or Thy1.1/2	Harty Lab	NA
<b>Software and algorithms</b>		
FlowJo v10.10.1 (with Downsample and UMAP plug-ins)	FlowJo, LLC	<a href="https://www.flowjo.com/solutions/flowjo/">https://www.flowjo.com/solutions/flowjo/</a>
Adobe Photoshop v21.0.3	Adobe	<a href="https://www.adobe.com/products/photoshop.html">https://www.adobe.com/products/photoshop.html</a>
ImageJ	Open Source	<a href="https://imagej.net/ij/">https://imagej.net/ij/</a>
Adobe Illustrator v24.0.1	Adobe	<a href="https://www.adobe.com/products/illustrator.html">https://www.adobe.com/products/illustrator.html</a>
Prism 10.1.1	Graphpad Software	<a href="https://www.graphpad.com/features">https://www.graphpad.com/features</a>
cellSens V4.2.1	Olympus Life Science	<a href="https://www.olympus-lifescience.com/en/software/">https://www.olympus-lifescience.com/en/software/</a>

(Continued on next page)

**Continued**

REAGENT or RESOURCE	SOURCE	IDENTIFIER
Other		
Hamilton 25 $\mu$ L Microliter Syringe Model 702 N, Cemented Needle, 22s gauge, 2 in, point style	2 Hamilton	Cat #80400
Epredia <sup>TM</sup> Peel-A-Way <sup>TM</sup> Disposable Embedding Molds	Thermo Fisher	Cat #22-19

**EXPERIMENTAL MODEL AND STUDY PARTICIPANT DETAILS****Mice**

Thy1.2 C57BL/6N mice were purchased from the National Cancer Institute. Thy1.1 P14 TCR-tg mice were a gift of Michael Bevan and were bred in-house at the University of Iowa Animal Care Facility. Mice used in all experiments were female and 6–10 weeks in age at the onset of experimentation. All animals were handled in accordance with guidelines established by the University of Iowa Institutional Animal Care and Use Committee. Mice were randomly assigned to experimental groups and mouse numbers within replicate experiments are reported in each figure legend.

**Adoptive transfer**

Thy1.1 P14 TCR-tg CD8<sup>+</sup> T cells were isolated from the blood or spleens of naive or 1M/2M/3M female donor mice. Spleens were dissociated through a 70  $\mu$ m filter. Red blood cells (RBCs) were lysed using 1X Vitalyse (CytoMedical Design Group) or ACK lysis buffer (in-house). For memory P14, single-cell suspensions were stained with anti-Thy1.1-PE in PBS with 5% fetal calf serum (FCS). PE-labeled P14s were eluted following positive enrichment with magnetic anti-PE beads (Miltenyi Biotec) as previously published.<sup>21,29</sup> Frequencies of TCR-tg cells were determined by flow cytometry. Naive P14 cells (10<sup>4</sup> for IAV infection; 6x10<sup>3</sup> for LCMV infection) or 1M/2M/3M P14 cells (10<sup>5</sup> for IAV infection; 6x10<sup>4</sup> for LCMV infection) were adoptively transferred via tail vein injection in a total volume of 200  $\mu$ L into recipient mice 1 day prior to infection.

**Infections**

Mice were infected with a 2 x 10<sup>4</sup> media tissue culture infectious dose (TCID<sub>50</sub>) of influenza A virus/PR/08/34 expressing GP<sub>33-41</sub> (IAV-GP33) in a total volume of 25  $\mu$ L I.N.<sup>77</sup> Alternatively, mice were infected with 2 x 10<sup>5</sup> plaque-forming units (PFU) lymphocytic choriomeningitis virus (LCMV) strain Armstrong in a total volume of 200  $\mu$ L I.P. Intracranial rechallenge was performed with 100 colony forming units (CFU) attenuated recombinant *Listeria monocytogenes* expressing GP<sub>33-41</sub> (att. rLM-GP33) or GAP50<sub>40-48</sub> (att. rLM-GAP50) delivered in a total volume of 10  $\mu$ L I.C.

**Antibody depletion and FTY720 treatment**

Mice received 1 dose of 2  $\mu$ g of a-Thy1.1 antibody (clone 19E12, BioXcell) I.P. to deplete Thy1.1 P14 T<sub>CIRCM</sub><sup>13</sup>. Mice received daily I.P. injections of 1 mg/kg FTY720 (Millipore Sigma) to block lymphocyte circulation.

**METHOD DETAILS****Tissue collection and cellular isolation**

Mice received an I.V. injection of 2  $\mu$ g anti-CD45 antibody (30-F11, BioLegend) conjugated to a fluorophore 3 minutes prior to tissue harvest during non-rechallenge conditions. Spleens were isolated and dissociated through a 70  $\mu$ m filter followed by red blood cell (RBC) lysis in ACK lysis buffer. For isolation of immune cells from the brain, tissue was isolated and digested in Collagenase/DNase for 45 min at 37°C. Brain tissue was then dissociated through a 70  $\mu$ m filter and separated using a layered 70% and 37% Percoll gradient spun at 2000 RPM for 20 min at 25°C. Brain mononuclear cells were collected at the gradient interface. For isolation of endothelial cells from the brain, tissue was isolated and digested with a mouse tumor dissociation kit (Miltenyi Biotec) and gentleMACS Octo Dissociator (Miltenyi Biotec). Brain tissue was then dissociated through a 70  $\mu$ m filter and separated using a debris removal kit (Miltenyi Biotec) spun at 3500 RPM for 10 min at 4°C. Brain mononuclear cells were collected as the pellet.

For brain fractionation, brains were extracted and placed in a dish containing cold 1X PBS. The ventricular spaces were opened using fine forceps to isolate the lateral, third, and fourth ventricle choroid plexus that were pooled together from 3 individual mice in the same experimental group. The ventricular spaces were washed into the PBS (representing the CSF fraction) and the solid parenchymal brain was placed into a separate well. Brain fractions were processed the same as whole brain tissue described above to generate single-cell suspensions.

**Cell staining and flow cytometry**

Single-cell suspensions were plated and surface stained for 30 min at 4°C with a panel of fluorescently labeled antibodies. Samples were then fixed with Cytofix (BD Bioscience) at 25°C for 10 min. Intracellular staining was performed using a FoxP3/Transcription

factor staining buffer kit (Tonbo Biosciences) at 25°C with a panel of fluorescently labeled antibodies. To assess cytokine production, single-cell suspensions were plated in the absence or presence of 200 nM GP<sub>33-41</sub> peptide with brefeldin A (BioLegend) for 5–6 hours at 37°C. Stimulated and unstimulated cells were similarly stained for surface markers at 4°C, permeabilized using a FoxP3 transcription factor staining kit (Tonbo), and stained for cytokines at 25°C. After staining, cells were transferred to 1.2 mL microtiter tubes (ThermoFisher) and approximately 15 µL of Count Bright Absolute Counting Beads were added to each tube (ThermoFisher). Flow cytometry data were acquired using an LSRFortessa (BD Bioscience) and analyzed using FlowJo software v.10 (FlowJo LLC) using Downsample and UMAP plug-ins.

#### **Immunohistochemistry**

Brain tissue was harvested fresh and rinsed with PBS to remove excess blood. Whole brains were submerged in 4% low-melting point agarose (Promega) within Peel-A-Way embedding molds (Thermo Fisher) and placed at 4°C to solidify. Embedded brain tissue was then sectioned in 150–200 µm sections using a Pelco easiSlicer vibratome (Ted Pella, Inc). Choroid plexus tissue was removed *en bloc* from the ventricles of separate brain specimens using fine forceps. Brain tissue sections and whole choroid plexus tissue were stained. Stained brain tissue was washed twice in PBS, fixed in 4% paraformaldehyde, washed again in PBS, and mounted on Superfrost Plus microscope slides (Fisher). After drying, slide coverslipping was performed with Prolong Gold Antifade Mountant with DAPI (ThermoFisher). Whole-slide images were acquired using a slide-scanning microscope (Olympus VS120) and reviewed in OlyVIA Software (Olympus). Image processing was performed in Adobe Photoshop (Adobe) and ImageJ.

#### **Bacterial counts**

For enumeration of rLM, halved brains were weighed and collected in 3 mL of 0.2% Igepal (Millipore Sigma) to be homogenized. The CFU/gram of tissue was determined by plating 10-fold serial dilutions on Tryptic Soy Broth (TSB)/streptomycin plates. Colony counts were determined after overnight plate incubation at 37°C.

#### **QUANTIFICATION AND STATISTICAL ANALYSIS**

Statistical details including number of mice, number of replicates, statistical tests, and statistical parameters can be found in respective figure legends. All statistical analyses were performed using GraphPad Prism (v10.0). When indicated, two-tailed unpaired student's t-tests were performed when comparing two independent groups, paired t-tests when comparing two paired groups, and one-way ANOVA with Tukey's multiple comparisons test when comparing more than two groups for one variable. In all cases,  $p < 0.05$  was set at statistical significance.  $p$  values are indicated in individual figures or in figure legends or are otherwise summarized as: \* $p < 0.05$ , \*\* $p < 0.01$ , \*\*\* $p < 0.001$ , \*\*\*\* $p < 0.0001$ .